Article

Cancer Cell

TIM-3 Regulates CD103$^+$ Dendritic Cell Function and Response to Chemotherapy in Breast Cancer

Graphical Abstract

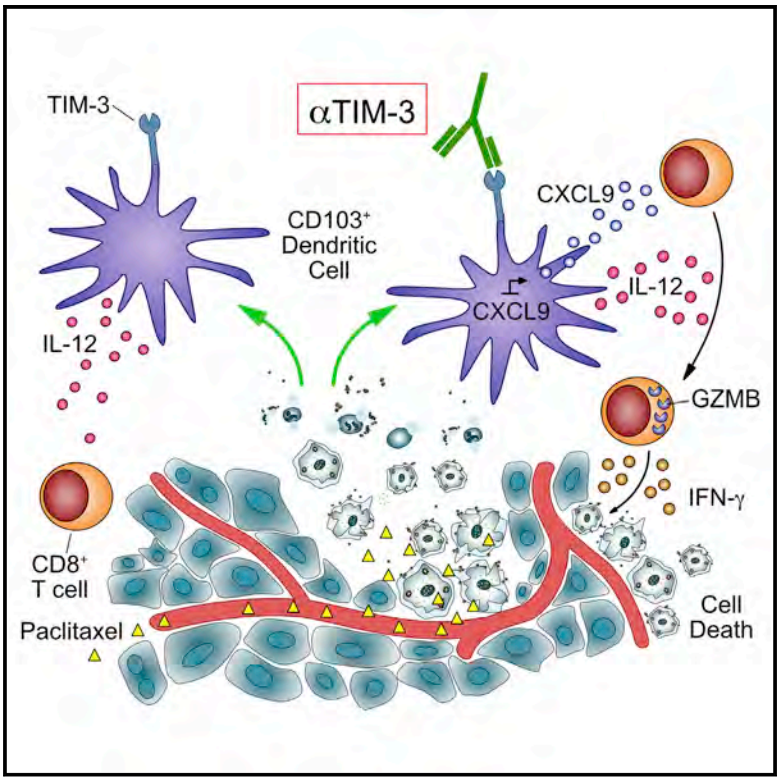

Authors

Álvaro de Mingo Pulido,
Alycia Gardner, Shandi Hiebler, ...,
Matthew F. Krummel,
Lisa M. Coussens, Brian Ruffell

Correspondence

brian.ruffell@moffitt.org

In Brief

de Mingo Pulido et al. show that intratumoral CD103$^+$ dendritic cells (DCs) highly express TIM-3. Anti-TIM-3 antibody promotes CXCL9 expression by these DCs, which enhances the function of CD8$^+$ T cells, thereby improving paclitaxel's therapeutic activity in breast cancer models.

Highlights

- TIM-3 is highly expressed by intratumoral CD103$^+$ dendritic cells
- TIM-3 antibody indirectly enhances a CD8$^+$ T cell response during chemotherapy
- TIM-3 antibody increases CXCL9 expression by dendritic cells
- CXCL9 expression correlates with response to chemotherapy in breast cancer

de Mingo Pulido et al., 2018, Cancer Cell *33*, 60–74
January 8, 2018
https://doi.org/10.1016/j.ccell.2017.11.019

CellPress

CellPress

Cancer Cell
Article

TIM-3 Regulates CD103$^+$ Dendritic Cell Function and Response to Chemotherapy in Breast Cancer

Álvaro de Mingo Pulido,[1] Alycia Gardner,[1,2] Shandi Hiebler,[1] Hatem Soliman,[1,3] Hope S. Rugo,[4] Matthew F. Krummel,[5] Lisa M. Coussens,[6] and Brian Ruffell[1,3,7,*]

[1]Department of Immunology, H. Lee Moffitt Cancer Center and Research Institute, 12902 Magnolia Drive SRB-2, Tampa, FL 33612, USA
[2]Cancer Biology PhD Program, University of South Florida, Tampa, FL 33620, USA
[3]Department of Breast Oncology, H. Lee Moffitt Cancer Center and Research Institute, Tampa, FL 33612, USA
[4]Department of Medicine and Helen Diller Family Comprehensive Cancer Center, University of California, San Francisco, CA 94143, USA
[5]Department of Pathology, University of California, San Francisco, CA 94143, USA
[6]Department of Cell, Developmental & Cancer Biology, and Knight Cancer Institute, Oregon Health & Science University, Portland, OR 97239, USA
[7]Lead Contact
*Correspondence: brian.ruffell@moffitt.org
https://doi.org/10.1016/j.ccell.2017.11.019

SUMMARY

Intratumoral CD103$^+$ dendritic cells (DCs) are necessary for anti-tumor immunity. Here we evaluated the expression of immune regulators by CD103$^+$ DCs in a murine model of breast cancer and identified expression of TIM-3 as a target for therapy. Anti-TIM-3 antibody improved response to paclitaxel chemotherapy in models of triple-negative and luminal B disease, with no evidence of toxicity. Combined efficacy was CD8$^+$ T cell dependent and associated with increased granzyme B expression; however, TIM-3 expression was predominantly localized to myeloid cells in both human and murine tumors. Gene expression analysis identified upregulation of *Cxcl9* within intratumoral DCs during combination therapy, and therapeutic efficacy was ablated by CXCR3 blockade, *Batf3* deficiency, or *Irf8* deficiency.

INTRODUCTION

The presence of cytotoxic CD8$^+$ T cells within tumors has a strong association with positive outcomes across a range of malignancies (Fridman et al., 2012), and they are important mediators of response to therapeutic interventions, including chemotherapy, radiotherapy, and targeted agents (Coffelt and de Visser, 2015). This is also true in breast cancer, and tumor-infiltrating lymphocytes are increasingly recognized as an emerging prognostic and predictive biomarker (DeNardo et al., 2011; Salgado et al., 2015). Enhancing the presence or functional activity of CD8$^+$ T cells is thus the central goal of most immunotherapies but despite recent successes, clinical response rates remain low and it has become increasingly clear that response correlates with mutational burden (Le et al., 2015; Rizvi et al., 2015; Van Allen et al., 2015) and the extent of an anti-tumor immune response prior to therapy initiation (Herbst et al., 2014; Tumeh et al., 2014). This a problem not only for individual patients, but also for tumor types that have a comparatively low mutational frequency and/or cytotoxic T cell response.

Conventional dendritic cells (cDCs) are well established as the central inducers of a T cell response through their ability to present antigenic peptides on major histocompatibility complex I (MHCI) and MHCII following activation/maturation. It is generally thought that migratory tumor DCs are required to prime a de novo T cell response within the draining lymph nodes (Chen and Mellman, 2013). These can be divided into two lineages in mice: the predominant CD11b$^+$ cDC2 population depends on the transcription factor interferon regulatory factor 4 (IRF4); while the minor CD8α/CD103$^+$ cDC1 population depends on the transcription factors IRF8 and basic leucine zipper transcription factor ATF-like 3 (BATF3) (Broz et al., 2014). Anti-tumor immunity

Significance

Immunotherapeutic approaches are particularly lacking in breast cancer, and thus we sought to identify potential therapeutic targets in a murine model. Herein we report that TIM-3 expression by intratumoral CD103$^+$ dendritic cells regulates chemokine expression during paclitaxel treatment, with anti-TIM-3 antibody administration leading to enhanced granzyme B expression by CD8$^+$ T cells and an immune-mediated response to chemotherapy. These findings expand upon the potential targets of TIM-3 antibodies currently in clinical trials, and offer a rationale for combinatorial studies with chemotherapy in breast cancer and other solid malignancies.

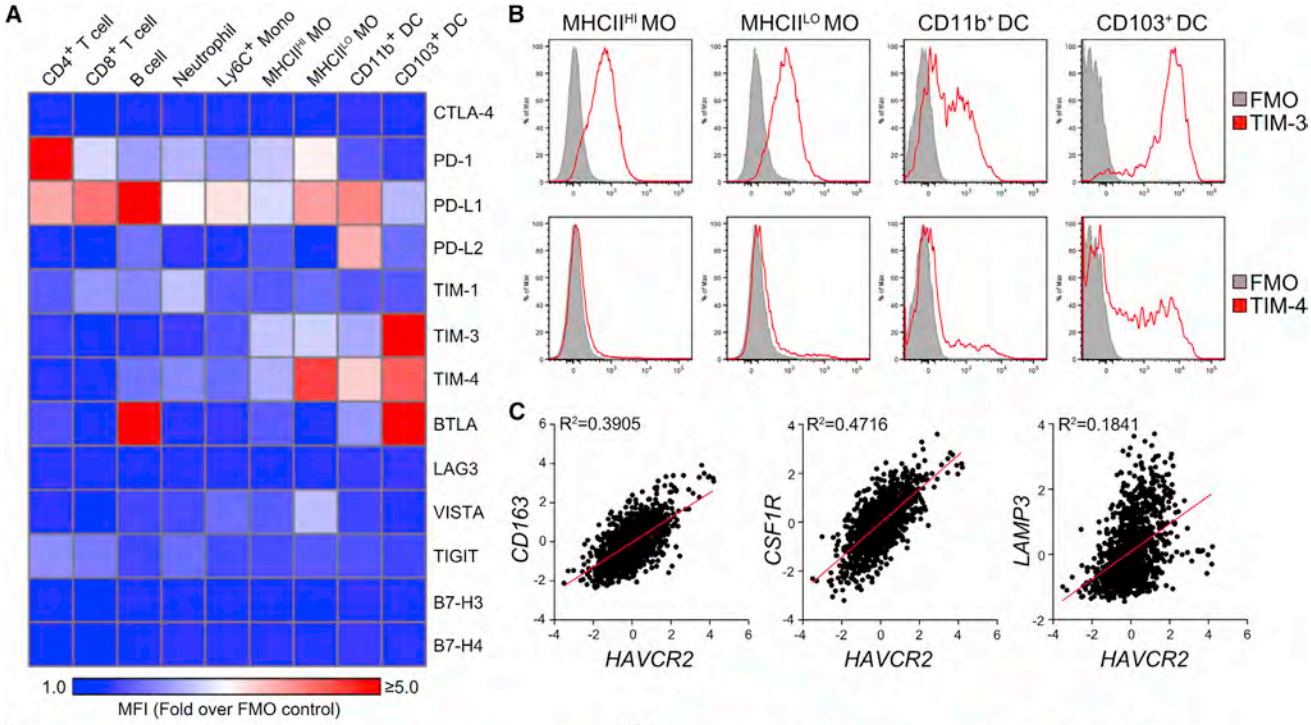

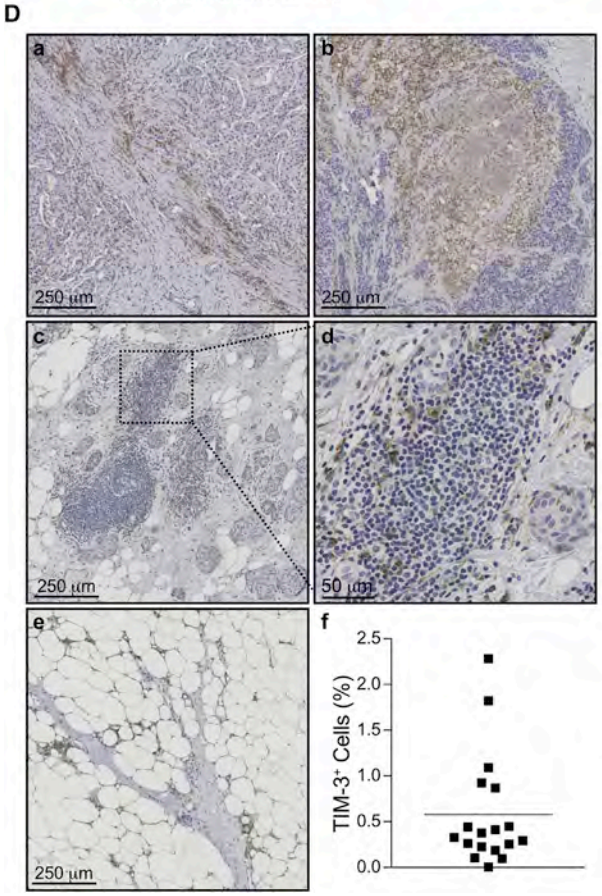

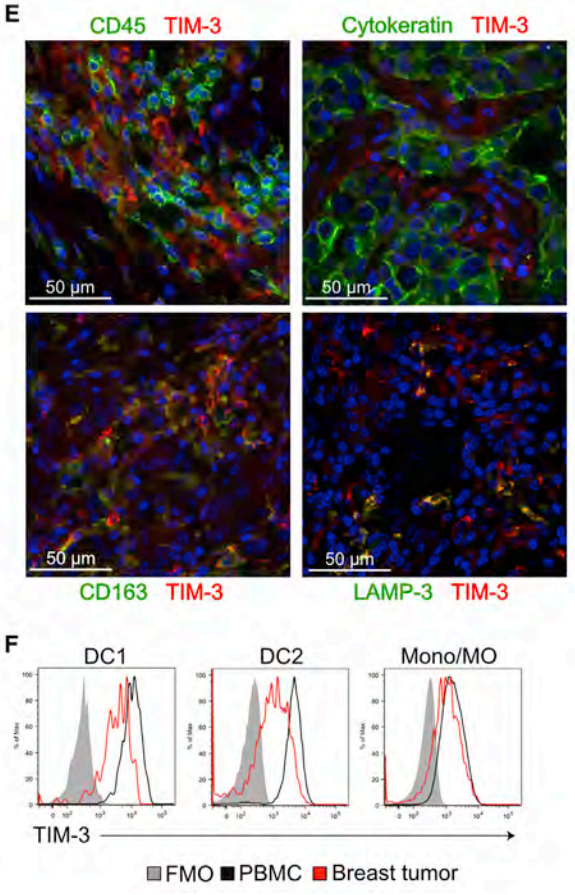

(legend on next page)

is absent in *Batf3*-deficient mice (Hildner et al., 2008; Sanchez-Paulete et al., 2015), and the recruitment of CD103$^+$ cDCs into tumors is necessary for a CD8$^+$ T cell response to develop (Spranger et al., 2015), implicating migratory CD103$^+$ cDCs as the inducers of a systemic CD8$^+$ T cell response under non-therapeutic conditions. This is consistent with their superior ability to transport and cross-present tumor antigens in the draining lymph nodes (Desch et al., 2011; Headley et al., 2016), including from spontaneously developing tumors (Roberts et al., 2016; Salmon et al., 2016).

In addition to their role in inducing *de novo* T cell responses, cDCs may be important in maintaining an effective T cell response within peripheral tissues (Iijima and Iwasaki, 2014; Natsuaki et al., 2014). Within tumors, CD103$^+$ cDC1s have also been shown to restimulate CD8$^+$ T cells and to mediate the efficacy of adoptive cell transfer therapy (Broz et al., 2014). Similarly, we have found that expression of interleukin-12 (IL-12) by CD103$^+$ cDC1s promotes a CD8$^+$ T cell response to chemotherapy following blockade of select immunosuppressive pathways (Ruffell et al., 2014). Based on these data, we therefore sought to determine whether tumor cDC1s could be therapeutically targeted through their expression of immune checkpoint molecules.

RESULTS

TIM-3 Is Highly Expressed by cDCs in Breast Cancer

To identify potential targets expressed by cDCs within tumors, we screened single-cell suspensions from transgenic mouse mammary tumor virus (MMTV)-PyMT mammary carcinomas by flow cytometry for surface expression of proteins associated with immune regulation (Figure 1A). Programmed death ligand-1 (PD-L1) was broadly expressed by leukocytes, and PD-1 was expressed by T lymphocytes; however, αPD-1 treatment had no effect on tumor growth alone or in combination with paclitaxel (PTX) (Figure S1A), consistent with previous findings in combination with radiotherapy (Bos et al., 2013).

In addition to PD-1/PD-L1 expression, we observed clustered expression of TIM-3 and TIM-4 on myeloid cells within tumors, particularly CD103$^+$ cDCs (Figure 1B). The gene for TIM-3, *HAVCR2*, also strongly correlated with macrophage-associated genes *CD163* and *CSF1R*, along with the DC-associated gene *LAMP3* in the TCGA dataset (Figure 1C). In contrast, *TIMD4* expression displayed poor correlation with these same genes (Figure S1B). Based on these data, we focused on analyzing the TIM-3 expression pattern in breast cancer using samples from 18 patients who had not received neoadjuvant therapy prior to surgical resection. TIM-3 cellular positivity by immunohistochemistry was found to be variable between individual tumors, ranging from over 2% to less than 0.1% (Figure 1D). Positive cells predominantly included those with a myeloid morphology in areas with high extracellular matrix deposition, cell death/necrosis, and invasive fronts. Based on the apparent staining of myeloid cells, we performed immunofluorescent staining in conjunction with pan-cytokeratin, CD45, CD163, or lysosomal associated membrane protein 3 (LAMP-3, DC-LAMP, CD208). TIM-3 was not observed on cytokeratin-expressing tumor cells (Figure 1E), and instead was largely observed on cells expressing lower levels of CD45, consistent with a myeloid localization. Indeed, TIM-3 showed a high degree of overlap with CD163$^+$ macrophages, with high TIM-3 expression also noted on LAMP-3^{HI} DCs. Expression by both CD141$^+$ cDC1 and CD1c$^+$ cDC2 populations within peripheral blood and breast tumors was confirmed using flow cytometry (Figures 1F, S1C, and S1D). These data demonstrate that TIM-3 is predominantly expressed by myeloid cells in breast and mammary carcinomas, and suggest that high expression of TIM-3 by cDCs could be a viable therapeutic target.

αTIM-3 Antibody Improves Response to Chemotherapy

As TIM-3 and TIM-4 were both expressed in the murine model, and combinatorial efficacy has been observed (Baghdadi et al., 2013), we first evaluated the effect of dual αTIM-3 and αTIM-4 antibodies in MMTV-PyMT transgenic mice. Although αTIM-3/αTIM-4 treatment alone did not alter tumor growth, in combination with PTX there was a significant reduction in growth for the duration of the experiment, as compared with treatment with PTX and an isotype control antibody (Figure 2A). These findings were extended to the C3(1)-TAg model of triple-negative breast cancer, where similar efficacy was observed in combination with PTX (Figure 2B). To determine which antibody was required, we individually combined them with PTX. αTIM-4 did not affect tumor growth, whereas αTIM-3 improved response to PTX equivalent to the combination of αTIM-3/αTIM-4 (Figure 2C). αTIM-3 also led to an increase in cell death within tumors compared with PTX alone, as seen by increased staining for cleaved caspase-3 (Figure S2A), and could improve response to the chemotherapeutic agent carboplatin, albeit not to the degree observed

Figure 1. TIM-3 Is Expressed by Tumor-Associated cDCs and Macrophages

(A) Surface expression of immune checkpoint markers on leukocyte populations within late-stage MMTV-PyMT tumors, as determined by flow cytometry. Results are shown as a heatmap of the mean fluorescence intensity (MFI) divided by the background of fluorescence-minus-one (FMO) controls. n = 3, one of three representative experiments shown. Mono, monocyte; MO, macrophage.

(B) Representative histograms from (A) displaying surface expression of TIM-3 and TIM-4 on macrophages and cDCs within MMTV-PyMT tumors.

(C) Correlation between *HAVCR2* expression and myeloid genes (*CD163*, *CSF1R*, *LAMP3*) in human breast cancer samples from the TCGA dataset (n = 1,161; R^2 values by linear regression).

(D) TIM-3 immunohistochemistry in human breast cancer tissue samples. Representative images from 18 patients display positive staining in stromal regions (a), necrotic areas (b), tertiary lymphoid structures (c and d), and adjacent normal tissue (e). Cellular positivity for TIM-3 is shown at (f), with the horizontal bar representing the mean.

(E) Immunofluorescent staining for TIM-3 (red) and CD45, cytokeratin, CD163, or LAMP-3 (green) in human breast cancer. DNA was visualized with Hoechst 33342 (blue). Three patient samples were analyzed for each combination.

(F) Representative histograms of TIM-3 expression by CD141$^+$ cDC1, CD1c$^+$ cDC2, or CD14$^+$ monocytes/macrophages in the peripheral blood of healthy volunteers (n = 5) or breast tumors (n = 9).

See also Figure S1.

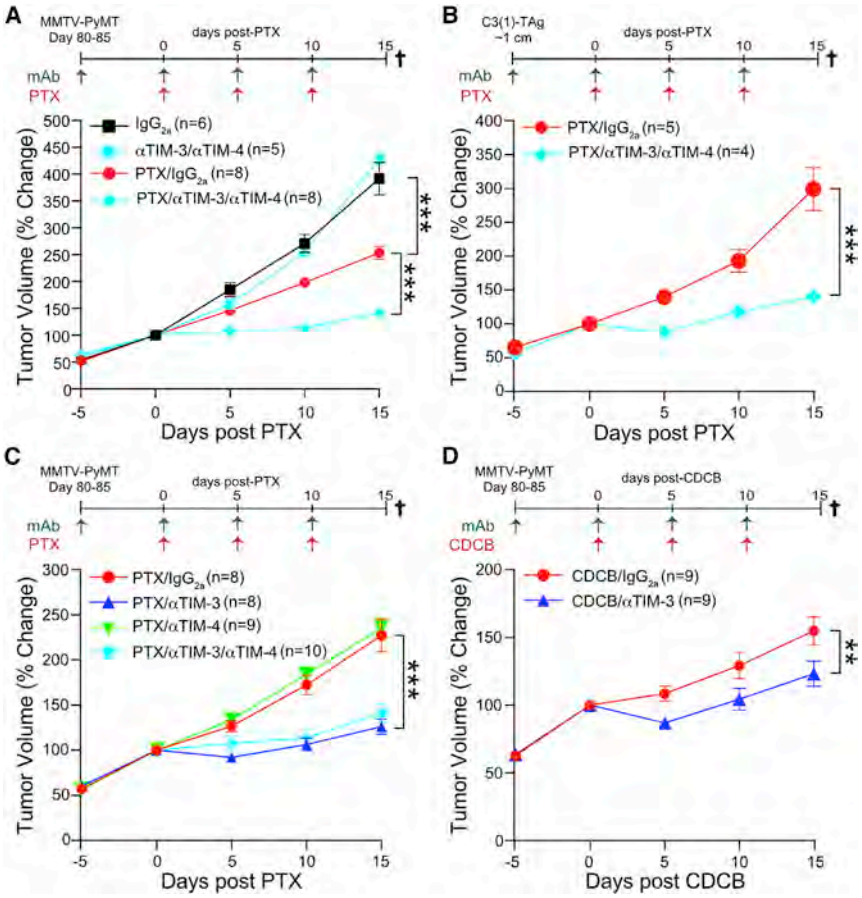

Figure 2. αTIM-3 Improves Response to Chemotherapy

(A) Tumor volume shown as a relative change from the initiation of chemotherapy (day 0) in MMTV-PyMT animals. Mice were treated with an immunoglobulin 2a (IgG_{2a}) isotype control or the combination of αTIM-3 and αTIM-4 antibodies, alone or together with 10 mg/kg PTX as indicated. n = 5–8 mice per group, pooled over four cohorts.

(B) Same as (A), except C(3)1-TAg animals were treated when a single tumor reached ~1 cm in diameter. n = 4–5 mice per group, pooled over four cohorts.

(C) Same as (A), except MMTV-PyMT animals were treated individually with αTIM-3 or αTIM-4 antibodies. n = 8–10 mice per group, pooled over four cohorts. Mice in the αTIM-3/αTIM-4/PTX group overlap with those in (A) and are shown for comparison.

(D) Same as (A), except MMTV-PyMT animals were treated with αTIM-3 in combination with 20 mg/kg carboplatin (CDCB). n = 9 mice per group, pooled over three cohorts.

Data are mean ± SEM; $^{**}p < 0.01$, $^{***}p < 0.001$, with statistical significance determined by two-way ANOVA. See also Figure S2.

with PTX (Figure 2D). Notwithstanding the effects of αTIM-3 on the primary tumor, there was no difference in the number or the size of the pulmonary metastatic foci in MMTV-PyMT animals across any of the treatment groups (Figure S2B). This failure to affect metastasis may relate to the late stage of intervention and/or the relative inability of $CD8^+$ T cells to suppress metastasis in the transgenic PyMT model (Bos et al., 2013; DeNardo et al., 2011). Importantly, however, αTIM-3 efficacy was not associated with clinical measures of toxicity as revealed by liver or kidney function tests (Figures S2C and S2D), thus demonstrating safety and efficacy against the primary tumor with the combination of αTIM-3 and PTX.

cDC1s Are Necessary for Response to αTIM-3

Although $CD103^+$ cDC1s expressed the highest levels of TIM-3 within tumors, it was possible that other TIM-3-expressing myeloid subsets were the actual targets of therapy. To confirm that cDC1s were functionally important, we acquired *Batf3* knockout animals and backcrossed them onto the FVB/NJ background. Only $Batf3^{+/-}$ MMTV-PyMT animals responded to αTIM-3, with no difference in tumor volume observed between $Batf3^{-/-}$ mice treated with immunoglobulin 2a (IgG_{2a})/PTX compared with αTIM-3/PTX (Figure 3A). Surprisingly, this phenotype was not due to the absence of $CD103/CD8\alpha^+$ cDC1 (Figure S3A), perhaps related to the secondary role of BATF3 in maintaining *Irf8*-dependent cDC development (Grajales-Reyes et al., 2015), and was instead most likely due to a defect in cross-presentation in *Batf3*-deficient cDCs (Jackson et al., 2011; Seillet et al., 2013). To clarify the importance of the cDC1 subset we generated *Itgax-cre*.$Irf8^{fl/fl}$ bone marrow chimeric animals on the C57BL/6J background, and confirmed the absence of cDC1s (Figure S3B). Following orthotopic implantation of syngeneic PyMT tumor cells, mice were treated with a combination of αTIM-3 and PTX, and as expected, *Itgax-cre*.$Irf8^{fl/fl}$ animals failed to respond to the combination therapy (Figure 3B).

A caveat to these findings is that mice lacking cDC1s prior to exposure to tumors would also be expected to lack an endogenous anti-tumor $CD8^+$ T cell response, making it unclear whether $CD103^+$ cDCs were the functional target of αTIM-3. We therefore created chimeric animals using donor *Zbtb46*-DTR bone marrow to allow depletion of cDCs after tumor implantation (Broz et al., 2014). Administration of diphtheria toxin preferentially depleted the $CD103^+$ cDC1 subset within tumors (Figure 3C) and prevented response to αTIM-3/PTX (Figure 3D). These results demonstrate that $CD103^+$ cDC1s are functionally necessary for response to therapy, and further support cDC1s being an important therapeutic target of TIM-3 blocking antibodies.

Despite the importance of cDC1s in mediating response to αTIM-3, infiltration by neither cDCs nor macrophages was altered by αTIM-3 administration, whether measured 2 or 5 days after PTX administration (Figures 3E and S3C). As TIM-3 has previously been reported to suppress intracellular TLR-induced activation of $CD11c^+$ myeloid cells (Chiba et al., 2012), we also examined whether the activation status of cDCs was altered within tumors from mice treated with αTIM-3/PTX. However, there was no difference in the surface expression of the activation/maturation markers CD80, CD86, CD40, MHCI,

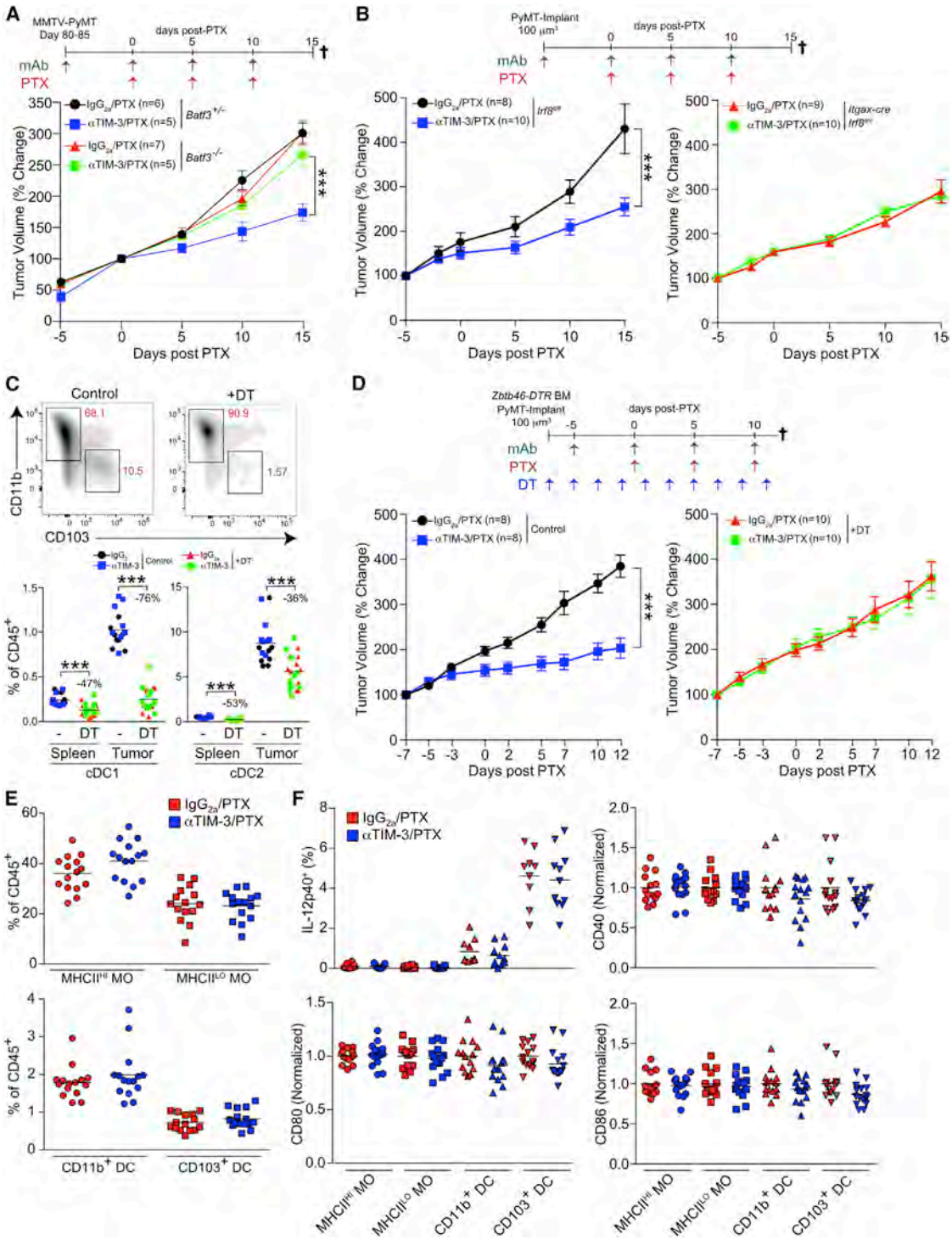

Figure 3. cDC1s Are Necessary for Response to αTIM-3

(A) Tumor volume shown as a relative change from the initiation of chemotherapy (days 0–15) in MMTV-PyMT animals either *Batf3* proficient (+/−) or *Batf3* deficient (−/−). Mice were treated with an IgG_{2a} isotype control or αTIM-3 antibody in combination with 10 mg/kg PTX as indicated. n = 5–7 per group, data pooled over five cohorts.

(B) Orthotopic PyMT tumor volume in chimeric C57BL/6J animals reconstituted with either *Itgax-cre.Irf8*$^{fl/fl}$ or *Irf8*$^{fl/fl}$ bone marrow. n = 8–10 per group, with one of two representative experiments shown.

(C) Top: cDC subsets (gated on $CD45^+CD11c^+MHCII^+F4/80^-$) within PyMT tumors of chimeric C57BL/6J animals reconstituted with *Zbtb46-DTR* bone marrow and treated with diphtheria toxin (DT) as indicated. Bottom: the percentage of each cDC subset within the spleens or tumors of mice treated as in (D). The percent reduction in the population resulting from DT administration is shown. n = 8–10 per group, with one of two representative experiments shown.

(legend continued on next page)

and MHCII, nor in expression of IL-12p40 by CD103$^+$ tumor cDC1s as measured by *ex vivo* intracellular staining (Figures 3F and S3D).

αTIM-3 Indirectly Promotes an Intratumoral CD8$^+$ T Cell Response

To determine whether αTIM-3 was enhancing a T cell response during PTX treatment, we began by evaluating whether CD4$^+$ or CD8$^+$ T cells were necessary for response to αTIM-3/PTX via depletion studies. CD4 depletion had no effect on response to therapy, while CD8 depletion prior to the initiation of chemotherapy prevented the improved response (Figure 4A). These studies were extended to determine the importance of cytokines implicated in promoting CD8/T_H1 responses to chemotherapy (Kroemer et al., 2013; Ruffell et al., 2014; Sistigu et al., 2014): obstructing type I interferon (IFN) signaling by blocking IFN-α receptor 1 (IFNAR1) abrogated the therapeutic effect of αTIM-3, a phenotype that was also observed when neutralizing antibodies against either IL-12p70 or IFN-γ were administered (Figure 4A). We next measured TIM-3 expression in tumor-bearing MMTV-PyMT animals and found that TIM-3 was not expressed on T lymphocytes in the blood, lymph node, or spleen (Figures 4B and 4C). TIM-3 was also barely detectable on CD8$^+$ T cells within most tumors, but was consistently expressed by about 20% of CD4$^+$ T cells (19.1% ± 1.3%). Minimal surface expression of TIM-3 by T cells was matched by lower expression of *Havcr2* compared with macrophages or cDCs (Figure S4A). Similarly, TIM-3 was not detectable on CD4$^+$ or CD8$^+$ T cells in breast cancer samples by immunofluorescence (Figure S4B). To better quantify expression on human T cells, we also analyzed TIM-3 expression by flow cytometry and, similar to murine mammary tumors, found only low expression by a small population of CD4$^+$ (8.1% ± 2.1%) and CD8$^+$ T cells (6.6% ± 3.1%) within breast tumors (Figures 4B and 4D). Therefore, while αTIM-3 enhances a CD8$^+$ T cell-dependent response to chemotherapy, the data indicate that this occurs via an indirect mechanism of action, consistent with high TIM-3 expression (Figure 1B) and the functional importance (Figures 3A–3D) of the cDC1 subset.

To differentiate between the induction of a systemic *de novo* immune response and enhancement of local effector function, we first evaluated the clonality of T cells within the peripheral blood, but observed no effect of αTIM-3 (Figure S4C). We then administered FTY720 to animals during the course of treatment to determine whether retention of T cells within the secondary lymphoid organs would prevent response to therapy. While, as expected, this retained T cells within the spleen and reduced the circulating population, it did not decrease infiltration by intratumoral T cells (Figure S4D), and no impact on tumor growth was observed in either the $IgG2_a$/PTX or αTIM-3/PTX treatment groups (Figure 4E). We therefore focused on identifying changes in T cells within tumors. There were no quantitative changes in tumor infiltration as a result of αTIM-3, regardless of whether tumors were examined 2 days or 5 days following PTX in the MMTV-PyMT transgenic model (Figures S4E and S4F), or in an orthotopic PyMT implantable model (Figure 4F). Expression of the T cell activation markers CD44 and CD69 by intratumoral T cells was highly variable between transgenic tumors but was similarly unchanged (Figure S4G). Given the high variability in T cell activation in the transgenic model, we evaluated T cell activation status in the PyMT implantable model, but again found no differences between treatment groups (Figure 4F). We next measured granzyme B within tumor T cells as a surrogate for cytotoxic potential using the PyMT implantable model and found that αTIM-3 in combination with PTX significantly increased the frequency of CD8$^+$ T cells expressing granzyme B, measured as either a percentage of total leukocyte infiltration or the total population of CD8$^+$ T cells (Figures 4G and S4H). A comparable increase in granzyme B expression was observed with αTIM-3/PTX treatment in MMTV-PyMT animals after controlling for the highly variable level of T cell activation (Figure 4H). *Ex vivo* activation and intracellular staining for IFN-γ and tumor necrosis factor α (TNF-α) also revealed a significant increase in the percentage of cells expressing these cytokines (Figure 4I).

αTIM-3 Increases CXCR3 Chemokine Ligand Expression by Tumor cDCs

As the data indicated that αTIM-3 improved the ability of CD103$^+$ cDC1s to enhance the effector function of CD8$^+$ T cells within tumors, we sought to identify a potential mechanism of action. Binding of phosphatidylserine (PS) to TIM-3 has been shown to promote uptake of antigens and cross-presentation by CD8α$^+$ cDC1s (Nakayama et al., 2009). Although in this case blockade of TIM-3 would be expected to suppress the induction of antitumor immunity, we examined the uptake of tumor antigens by flow cytometry using transgenic FVB/NJ animals expressing PyMT, mCherry, and ovalbumin under the control of the MMTV promoter (i.e., PyMTchOVA). As previously reported, macrophages were the dominant antigen-presenting population within tumors, with both CD11b$^+$ and CD103$^+$ cDC1 subsets displaying lower levels of mCherry uptake (Broz et al., 2014). However, no difference was observed between mice treated with αTIM-3 versus an isotype control in terms of the percentage of cells or their overall fluorescence (Figure 5A).

To take a more unbiased approach in determining how cDC1s were altered by αTIM-3, we isolated macrophages and cDCs from orthotopically implanted PyMT tumors (to minimize the impact of variation inherent in the transgenic model), and performed gene expression analysis using the NanoString nCounter Mouse Immunology Panel. Significant changes ($p < 0.05$) that exceeded 1.5-fold between animals treated with αTIM-3/PTX

(D) Tumor volume in chimeric C57BL/6J animals reconstituted with *Zbtb46-DTR* bone marrow and treated with DT as indicated. n = 8–10 per group, with one of two representative experiments shown.

(E) Frequency of macrophage (MO) and cDC subsets as a percentage of total CD45$^+$ cells within tumors of MMTV-PyMT animals treated with PTX and αTIM-3 antibody, determined by flow cytometry (day 7). n = 15 per group, data pooled over three cohorts.

(F) Intracellular flow-cytometric analysis of IL-12p40, along with surface expression of CD40, CD80, and CD86 on macrophages and cDCs from MMTV-PyMT animals treated with PTX in conjunction with IgG_{2a} or αTIM-3 (day 7). n = 13–15 per group, data pooled over three experiments by normalizing to 1 as indicated. Data in (A), (B), and (D) are shown as mean ± SEM; ***$p < 0.001$, with significance determined by two-way ANOVA. Horizontal bars in (C), (E), and (F) represent the mean; ***$p < 0.001$, with significance determined by unpaired t test. See also Figure S3.

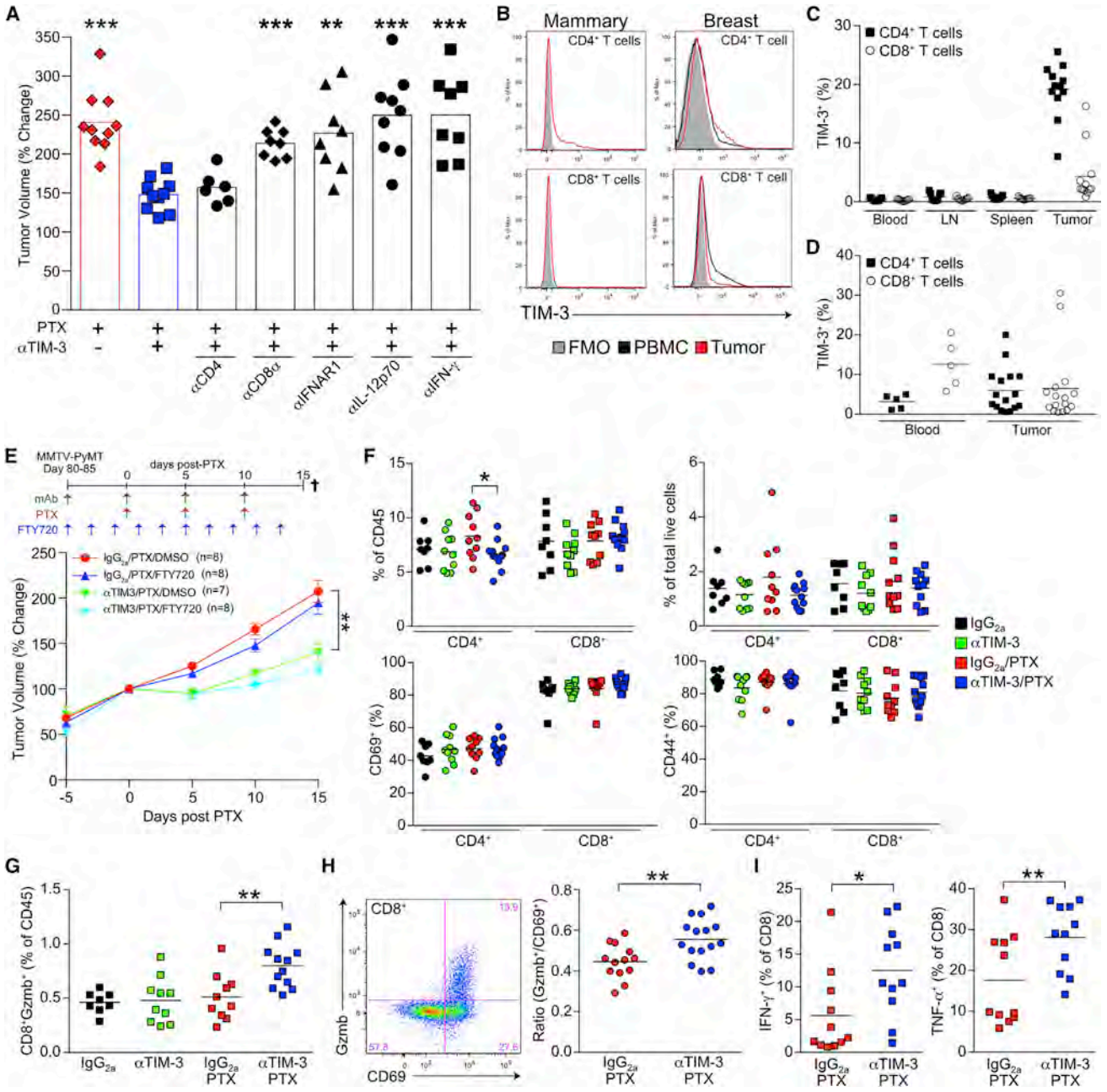

Figure 4. αTIM-3 Indirectly Enhances a CD8⁺ T Cell Response

(A) Relative tumor volume after three rounds of PTX in MMTV-PyMT transgenic mice (day 15). Blocking (αIFNAR1), neutralizing (αIL-12p70, αIFN-γ), and depleting (αCD8α, αCD4) antibodies were administered concurrently with αTIM-3, 5 days prior to and then in conjunction with PTX every 5 days. n = 8–12 per group, data pooled over seven cohorts. Bar graphs represent the mean; $^{**}p < 0.01$, $^{***}p < 0.001$, with significance determined by an unpaired t test with Welch's correction compared with αTIM-3.

(B) Representative histograms of TIM-3 surface expression on T cells from MMTV-PyMT animals (left) or human breast tumors (right).

(C) TIM-3 expression on murine T cells from MMTV-PyMT animals shown as a percentage of the total positive cells. n = 9–12 per tissue, data merged from three experiments.

(D) Percentage of TIM-3⁺ human T cells in the peripheral blood of healthy volunteers (n = 5) or within breast tumors (n = 16).

(E) Relative tumor volume in MMTV-PyMT animals treated with IgG_{2a}/PTX or αTIM-3/PTX in combination with FTY720 or DMSO as indicated. n = 7–8 mice per group, pooled over four cohorts. Data shown as mean ± SEM; $^{**}p < 0.01$, with significance determined by two-way ANOVA.

(F) Frequency of CD8⁺ and CD4⁺ T cells within tumors as a percentage of total CD45⁺ (top left) or live cells (top right), and the percentage of T cells expressing CD69 (bottom left) or CD44 (bottom right) in tumors.

(G) CD8⁺Gzmb⁺ T cells shown as percentage of total leukocyte infiltration.

(legend continued on next page)

and IgG_{2a}/PTX are shown in Figure S5A. $CD103^+$ cDC1s displayed increased expression of only five genes (*Cxcl11*, *Cxcl10*, *Cxcl9*, *Tagap*, and *Cd40*), with a corresponding increase in chemokine expression also observed in $CD11b^+$ cDCs (Figure 5B). As *Cxcl9* was expressed at much higher levels in cDCs than *Cxcl10* or *Cxcl11* (more than 10-fold in $CD103^+$ cDC1), we next examined whether CXCL9 could be detected at the protein level within tumor leukocytes. In transgenic MMTV-PyMT tumors CXCL9 was only detectable in $CD103^+$ cDCs isolated directly from mice following *in vivo* administration of brefeldin A (Figure 5C), consistent with preferential expression of *Cxcl9* mRNA by this subset (Figure S5B). Only following *ex vivo* stimulation with IFN-γ could CXCL9 be detected in all of the myeloid subsets examined (Figure S5C). Based on the increase in *Cxcl9* expression and specific expression of CXCL9 by $CD103^+$ cDC1s *in vivo*, a blocking antibody against CXCR3 (receptor for CXCL9, CXCL10, and CXCL11) was administered during combination therapy whereby, as shown in Figure 5D, blocking CXCR3 abrogated the effect of αTIM-3. Similar results were obtained with a specific inhibitor of CXCR3 (Figure 5E) that blocked migration of activated splenic $CD8^+$ T cells toward either CXCL9 or CXCL10 *in vitro* (Figure S5D). Cumulatively, these data point to a potential role for CXCL9-expressing $CD103^+$ cDC1s in promoting a cytotoxic T cell response following TIM-3 blockade.

αTIM-3 and αGalectin-9 Antibodies Promote CXCL9 Expression

To determine whether αTIM-3 could directly regulate CXCL9 expression, bone marrow DCs (BMDCs) were first generated using Fms-related tyrosine kinase 3 ligand (FLT-3L). However, these cells only expressed low levels of TIM-3 (Figure S6A) and, despite previous reports (Chiba et al., 2012), we did not find that IL-10 or vascular endothelial growth factor A increased TIM-3 expression *in vitro* (Figures S6B and S6C). In addition, blockade of the IL-10 receptor had no effect on TIM-3 expression on macrophages or cDCs within MMTV-PyMT tumors (Figure S6D), indicating that this pathway was not a major driver of TIM-3 expression by tumor myeloid cells. We therefore enriched for splenic cDCs, as $CD8\alpha^+$ cDC1s displayed expression levels of TIM-3 comparable with that of tumor $CD103^+$ cDC1s (Figure S6E), and stimulated the cells with poly(I:C) or CpG in the presence or absence of αTIM-3. However, neither TLR ligand increased CXCL9 expression, and there was no impact of αTIM-3 on CXCL9 or IL-12 expression in either cDC subset (Figure 6A). As these agonists do not reflect the ligands that would be present with tumors, we next utilized the supernatant of PyMT tumor cells killed by irradiation or heat shock *in vitro*. Tumor cell debris alone had little to no impact on CXCL9 expression; however, CXCL9 expression was consistently enhanced in $CD8\alpha^+$ cDC1s by the addition of the αTIM-3, with a small increase also observed for $CD11b^+$ cDC2s (Figure 6B). This was consistent with the increase in *Cxcl9* mRNA expression we observed within tumor $CD103^+$ cDC1s (Figure 5B). We also found no increase in expression of surface activation markers in response to tumor cell debris *in vitro* (Figure S6F), similar to our *in vivo* observations (Figures 3F and S3D). Together, these results suggest that TIM-3 can directly regulate CXCL9 expression by $CD103^+$ cDC1s within tumors.

We next sought to evaluate whether neutralizing antibodies against identified TIM-3 ligands (Anderson et al., 2016) could recapitulate the increase in CXCL9 expression observed with αTIM-3. As shown in Figure 6C, neither antibodies against high-mobility group box 1 (αHMGB1) nor αCEACAM1 affected CXCL9 expression, while αGalectin-9 led to an increase comparable to that with αTIM-3. Galectin-9 was found on the surface of all cells examined within MMTV-PyMT tumors, including epithelial cells, fibroblasts, and leukocytes (Figure 6D). Similarly, galectin-9 was found throughout human breast tumors, with strong staining within the stromal regions by immunohistochemistry, and variable levels of staining observed in carcinoma cells (Figures S6G and S6H). We therefore examined whether galectin-9 neutralization could improve response to PTX, and found that αGalectin-9 was equivalent to αTIM-3 in suppressing tumor growth during PTX treatment (Figure 6E). The efficacy of αGalectin-9/PTX was also $CD8^+$ T cell- and CXCR3-dependent (Figure 6F). While both TIM-3 and galectin-9 have multiple potential binding partners, the data suggest that an interaction between these molecules may be involved in regulated the function of cDCs within tumors.

DC Infiltration Correlates with *CXCL9* Expression and Response to Chemotherapy

Murine cDC1s expressed TIM-3 (Figure 1B) and were an important source of CXCL9 within mammary tumors (Figures 5C and S5B). As human cDC1s constitutively expressed TIM-3 (Figures 1F and S1D), we next sought to determine whether they might also be an important source of CXCL9 within breast tumors. Indeed, *CXCL9* gene expression correlated with expression of both *LAMP3* and *IRF8* (R^2 = 0.5884; R^2 = 0.4834), consistent with expression by the human cDC1 equivalent, while displaying minimal correlation with *CSF1R* or *IRF4* (R^2 = 0.1202; R^2 = 0.2084) (Figures 7A and S7A). Similarly, CXCL9 expression was detected by immunofluorescence in $LAMP3^+$ DCs but not $CD163^+$ macrophages (Figure 7B). Thus, both human and murine cDC1s express TIM-3 and CXCL9, suggesting that αTIM-3 antibodies may be a viable method to enhance the function of cDCs in breast cancer.

HAVCR2 gene expression in tumors was largely due to expression by macrophages (Figures 1C–1E), and therefore was not useful as a marker of cDCs or the importance of TIM-3 expression by this population. We thus examined whether *CXCL9* expression correlated with the presence of cytotoxic T cells, and observed an association with both *CD8A* and *GZMB* (Figure 7C). These associations were largely consistent across molecular subtypes (Figures S7B and S7C). We have

(H) Ratio of $CD8^+Gzmb^+$ to $CD8^+CD69^+$ T cells in tumors from MMTV-PyMT animals treated with IgG_{2a}/PTX or αTIM-3/PTX (day 7). n = 13–15 per group, data pooled over three cohorts. Representative staining for CD69 and Gzmb is shown on the left.

(I) Percentage of IFN-γ- or TNF-α-expressing $CD8^+$ T cells.

Data for (F), (G), and (I) are from mice bearing PyMT implantable tumors treated with IgG_{2a}, αTIM-3, or PTX (day 7). n = 8–12 per group, data pooled from two experiments. Horizontal bars in (C), (D), and (F) to (I) represent the mean; *$p < 0.05$, **$p < 0.01$, with significance determined by unpaired t test. See also Figure S4.

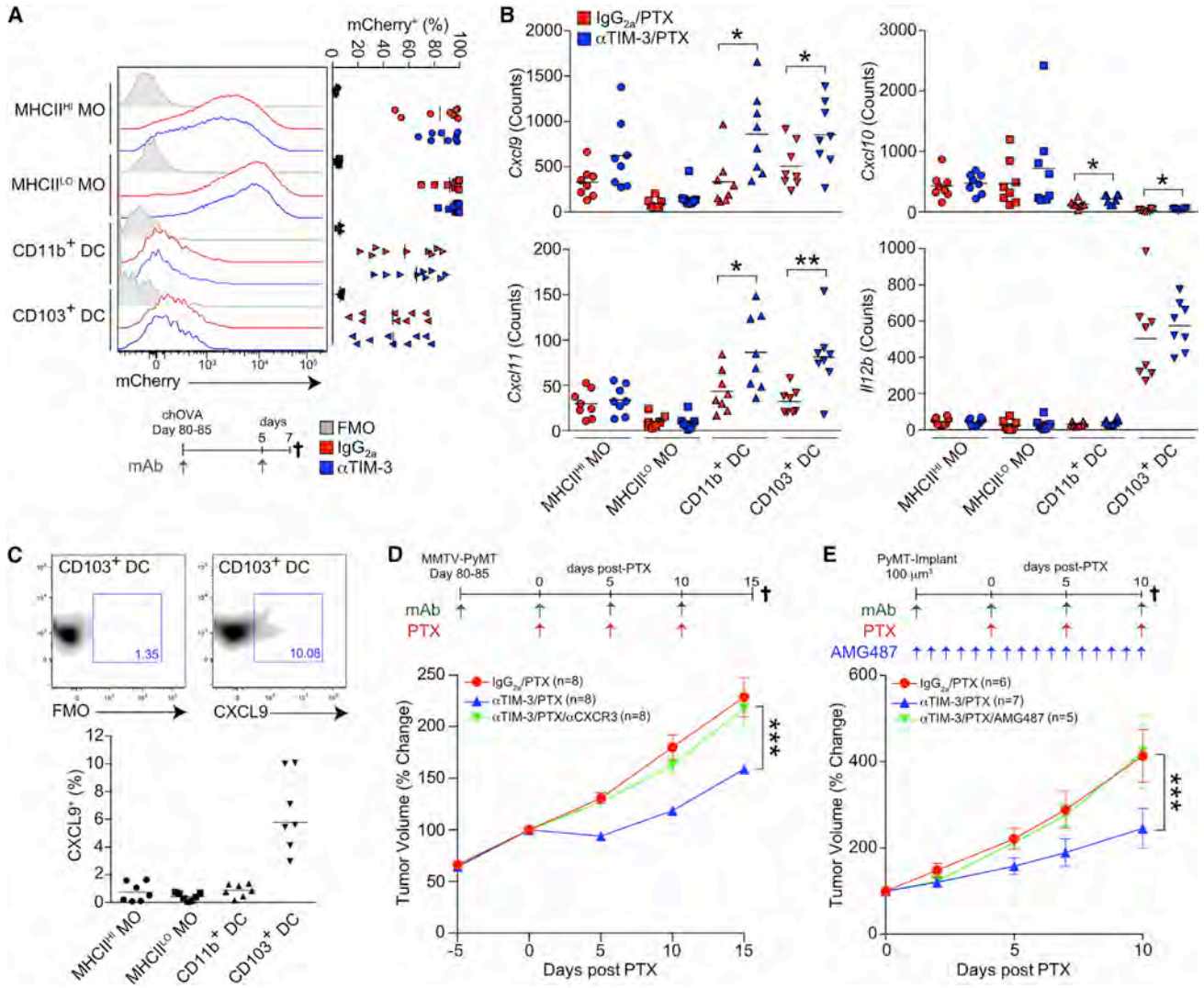

Figure 5. αTIM-3 Increases CXCR3 Ligand Expression by cDCs

(A) Detection of mCherry fluorescence in macrophages and cDCs from PyMTchOVA tumors. Mice were treated with isotype control or αTIM-3 for 7 days prior to analysis. n = 9 per group, data pooled over five experiments.

(B) mRNA expression levels in tumor macrophages and cDCs isolated from mice bearing orthotopically implanted PyMT tumors 2 days following the second dose of PTX (day 7). Expression of *Cxcl9*, *Cxcl10*, *Cxcl11*, and *Il12b* was determined by NanoString, with normalized counts displayed. n = 8 per group, data pooled from two experiments.

(C) Intracellular flow-cytometric analysis of CXCL9 in macrophages and cDCs from MMTV-PyMT animals following intravenous injection of brefeldin A for 4–6 hr. Representative staining as well as a fluorescence-minus-one (FMO) control is shown above. n = 7, data pooled over two experiments.

(D) Tumor volume shown as a relative change from the initiation of chemotherapy (day 0) in MMTV-PyMT animals. Mice were treated with an IgG_{2a} isotype control, αTIM-3, and/or αCXCR3 antibodies, together with 10 mg/kg PTX as indicated. n = 8 mice per group, pooled over four cohorts.

(E) Orthotopic PyMT tumor volume in C57BL/6J animals treated with an IgG_{2a} isotype control, αTIM-3, and/or (±)-AMG 487, together with 10 mg/kg PTX as indicated. n = 5–7 per group, with one of two representative experiments shown.

Horizontal bars in (A) to (C) represent the mean; *p < 0.05, **p < 0.01, with significance determined by unpaired t test. Data in (D) and (E) are shown as mean ± SEM; ***p < 0.001, with significance determined by two-way ANOVA. See also Figure S5.

previously described that expression of *CD8A* or *GZMB* is associated with a higher rate of pathological complete response to chemotherapy in breast cancer patients (Ruffell et al., 2014) using published datasets (Hess et al., 2006; Tabchy et al., 2010). We therefore evaluated whether the same was true for *LAMP3* or *CXCL9* and found a comparable ~2-fold segregation in response rates for each gene (Figure 7D). Similarly, *CD8A*, *LAMP3*, and *CXCL9* expression all correlated with recurrence-free survival in patients with basal or Her2 disease subtypes (Figures 7E and S7D). Collectively these data hint at an important role for cDC1s in promoting a cytotoxic T cell response through CXCL9 production, and suggest that αTIM-3 antibodies could enhance this expression, promote response to neoadjuvant chemotherapy, and improve survival.

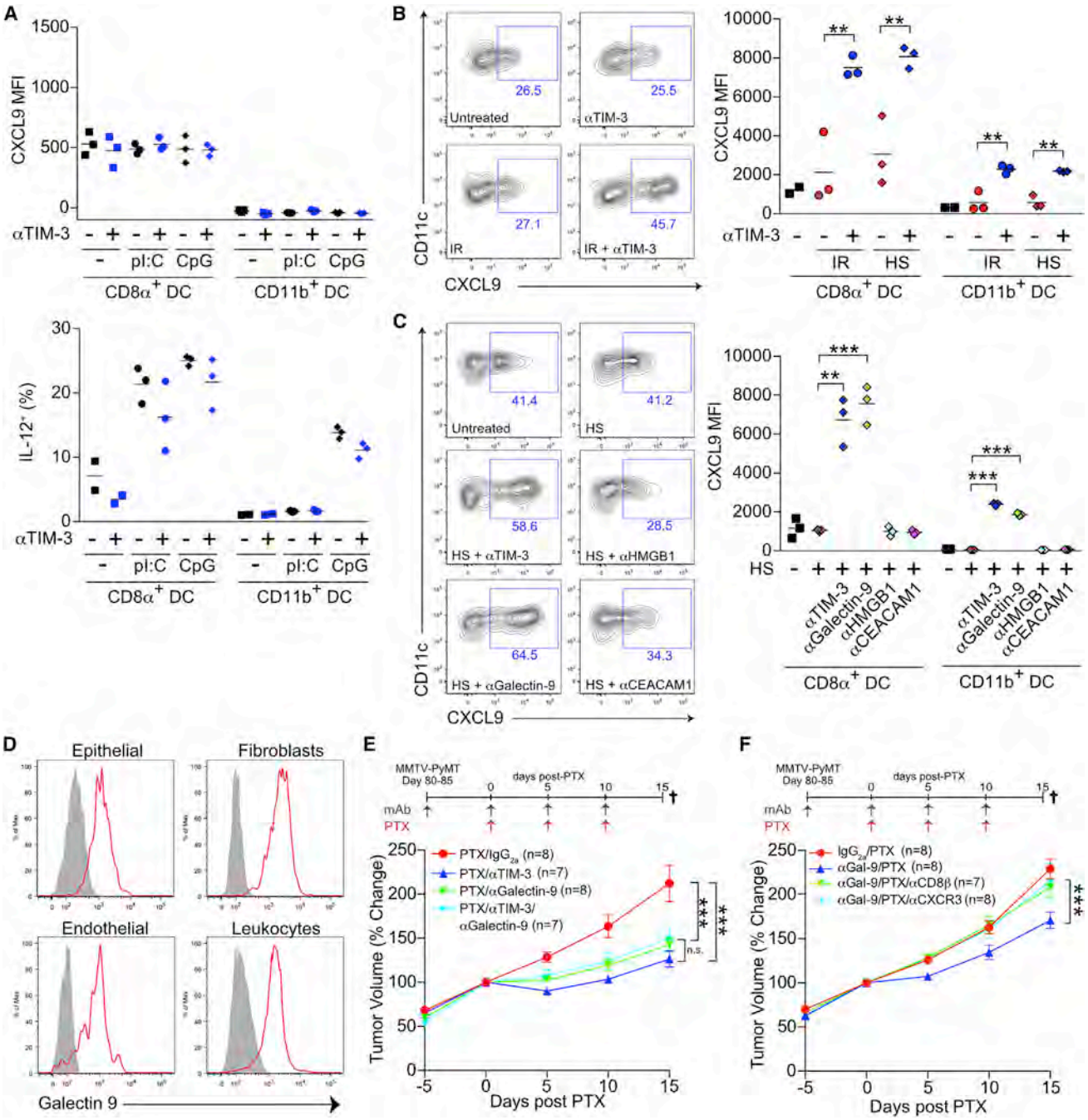

Figure 6. αTIM-3 and αGalectin-9 Antibodies Promote CXCL9 Expression

(A) CXCL9 (top) or IL-12 (bottom) expression by splenic cDCs following stimulation with Poly(I:C) (pI:C) or CpG (1 μg/mL). One of two representative experiments is shown.

(B) CXCL9 expression by splenic cDCs following incubation with αTIM-3 and/or tumor cell debris generated by irradiation (IR) or heat shock (HS). One of three representative experiments is shown.

(C) Same as (B), but with αTIM-3, αGalectin-9, αHMGB1, or αCEACAM-1 antibodies added in combination with tumor cell debris generated by HS. One of two representative experiments is shown.

(D) Detection of galectin-9 on the surface of EpCAM$^+$ epithelial cells, PDGFRα$^+$ fibroblasts, CD31$^+$ endothelial cells, or CD45$^+$ leukocytes from MMTV-PyMT tumors, as determined by flow cytometry. Gray histograms represent FMO control. n = 3, one of three representative experiments shown.

(E) Tumor volume shown as a relative change from the initiation of chemotherapy (day 0) in MMTV-PyMT animals. Mice were treated with an IgG_{2a} isotype control or the combination of αTIM-3 and αGalectin-9 antibodies, alone or together with 10 mg/kg PTX as indicated.

(legend continued on next page)

DISCUSSION

TIM-3 was originally identified based on its preferential expression by T_H1-polarized $CD4^+$ T cells, and αTIM-3 antibodies can promote T_H1-responses by reducing cell death and exhaustion in autoimmunity and infection models (Kane, 2010; Monney et al., 2002). TIM-3 expression is also associated with an exhausted phenotype in $CD8^+$ T cells during chronic infection, graft-versus-host disease, and cancer, and TIM-3 blockade increases IFN-γ expression *in vivo* and *ex vivo* (Jin et al., 2010; Jones et al., 2008; Oikawa et al., 2006; Sakuishi et al., 2010). Cumulatively these studies have led to interest in developing therapeutic antibodies against TIM-3 to enhance T cell immunity. Within MMTV-PyMT tumors, TIM-3 was expressed by a fraction of $CD4^+$ T cells, consistent with previous reports using subcutaneously implanted cell lines (Ngiow et al., 2011; Sakuishi et al., 2010). However, CD4 depletion had no effect on response to combination therapy with αTIM-3 and PTX, indicating that any effects on this population were irrelevant in our model. We were unable to detect TIM-3 on $CD8^+$ T cells within most MMTV-PyMT tumors, despite expression on a large proportion of $CD8^+$ T cells in the subcutaneous tumor models mentioned above (Ngiow et al., 2011; Sakuishi et al., 2010). These differences may reflect the intensity of an antigen-specific response, as TIM-3 expression by $CD8^+$ T cells is associated with antigen specificity in melanoma patients (Baitsch et al., 2011; Fourcade et al., 2010), and transgenic tumor models show a lower frequency of neo-epitopes (Yadav et al., 2014). Breast tumors also display a lower average frequency of somatic mutations (Alexandrov et al., 2013), and our findings in mice were consistent with our observations in human breast tumors. Despite the paucity of TIM-3 on the surface of $CD8^+$ T cells, they were required for response to αTIM-3 combination therapy. Thus, αTIM-3 antibodies can promote T cell immunity without directly targeting T cells, a finding that has implications for clinical trial design and patient selection criteria, for example, by not restricting treatment to only patients who display TIM-3^+ lymphocytes.

Instead of T cells, we found that TIM-3 expression was localized to macrophages and cDCs in tumors and normal tissues, with the highest levels consistently found on the cDC1 subset. We are far from the first to describe TIM-3 expression by myeloid cells under homeostatic conditions, as TIM-3 is found on mast cells, monocytes, microglia, splenic cDCs, and human circulating cDCs (Anderson et al., 2007; Nakayama et al., 2009; Phong et al., 2015). Inflammation-induced TIM-3 expression by peritoneal macrophages and microglia has also been observed, though not in human glioblastoma multiforme (Anderson et al., 2007; Nakayama et al., 2009). Finally, $CD11c^+$ cells within subcutaneous murine tumors express TIM-3, although whether these represent macrophages or cDCs is unclear, and TIM-3 expression by $CD11c^+$ cells was not apparent in the spleens or lymph nodes from the same study (Chiba et al., 2012), despite previous reports and our own observations (Nakayama et al., 2009).

Little is understood regarding the molecular mechanisms by which TIM-3 regulates immune responses. In T cells, galectin-9 binding induces tyrosine phosphorylation and prevents an association with nuclear factor HLA-B-associated transcript 3 (Rangachari et al., 2012; van de Weyer et al., 2006; Zhu et al., 2005). However, TIM-3 expression has also been shown to enhance early T cell receptor signaling and promote acute $CD8^+$ T cell responses (Gorman et al., 2014; Lee et al., 2011). Similarly, antibodies against TIM-3 can both suppress and induce nuclear factor κB activation in BMDCs and DC cell lines, respectively (Anderson et al., 2007; Maurya et al., 2014), and have been shown to promote Fc receptor signaling in mast cells (Phong et al., 2015). Some of these differences might relate to the fact that TIM-3 is not the only receptor for galectin-9 (Katoh et al., 2007; Su et al., 2011), or that as galectin-9 binds to carbohydrate moieties on TIM-3, protein expression alone does not ensure that binding will occur (Leitner et al., 2013). Furthermore, as TIM-3 is also a receptor for PS, HMGB1, and CEACAM-1, there may be important interplay between these ligands under pathological conditions such as those found within tumors. Finally, while the RMT3-23 antibody clone used in this study has been shown to block TIM-3 binding to galectin-9, PS, and HMGB1 (Chiba et al., 2012; Kanzaki et al., 2012; Nakayama et al., 2009), it remains possible that RMT3-23 could directly induce tyrosine phosphorylation, as has been described for polyclonal antibodies and other αTIM-3 antibody clones (Maurya et al., 2014; Phong et al., 2015). The mechanism by which αTIM-3 antibody promotes CXCL9 expression by cDCs is currently under investigation.

It has recently been described that $CD103^+$ cDC1s are necessary to promote antigen-specific T cell recruitment into immunogenic melanoma tumors through their ability to express CXCL10 (Spranger et al., 2017). In contrast, in mammary tumors we found that $CD103^+$ cDC1s expressed minimal levels of *Cxcl10*, and instead expressed the highest levels of *Cxcl9* when compared with other leukocyte subsets within tumors. Despite the increase in *Cxcl9* expression observed following αTIM-3/PTX treatment, however, we did not detect an increase in T cell infiltration. This may be due to expression of multiple T cell-attracting chemokines within tumors (e.g., CCL5, CXCL9, and CXCL10), or selective recruitment of antigen-specific cells that is not detected when measuring bulk T cell infiltration. Alternatively, as FTY720 administration did not affect response to αTIM-3/PTX, it may be that local promotion of a $CD8^+$ T cell effector response explains our observations. Interestingly, CXCL9 expression by cDCs has previously been described to mediate DC-T cell clustering within lymph nodes (Kastenmuller et al., 2013), and as DC-T cell interactions are infrequent within tumors (Broz et al., 2014), it is possible that increased expression of CXCL9 could facilitate these

(F) Same as (E), but mice were treated with αGalectin-9/PTX alone or with αCXCR3 or αCD8β antibodies.

Horizontal bars in (A) to (C) represent the mean of technical replicates; $^{**}p < 0.01$, $^{***}p < 0.001$, with significance determined by an unpaired t test. Data in (E) and (F) represent 7–8 mice per group, pooled over four cohorts, and are shown as mean ± SEM; $^{***}p < 0.001$, with significance determined by two-way ANOVA. See also Figure S6.

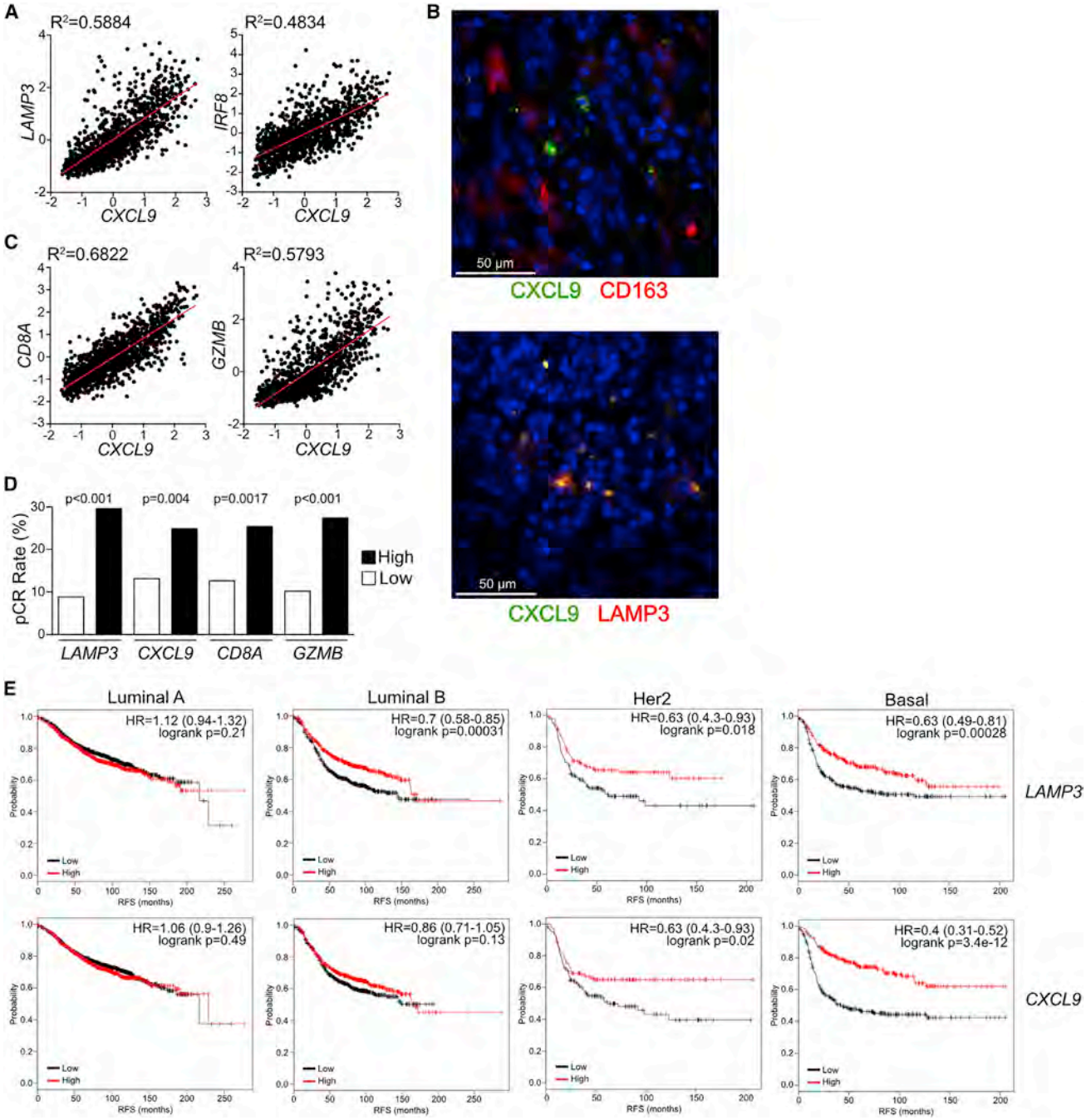

Figure 7. DC Infiltration Correlates with *CXCL9* Expression and Response to Chemotherapy

(A) Linear regression analysis between *CXCL9* expression and DC-associated genes (*LAMP3*, *IRF8*) in human breast cancer samples from the TCGA dataset (n = 1,161).

(B) Immunofluorescent staining for CXCL9 (green) and CD163 or LAMP3 (red) in human breast cancer. DNA was visualized with Hoechst 33342 (blue). Three patient samples were analyzed for each combination.

(C) Linear regression analysis between *CXCL9* expression and various cytotoxic lymphocyte-associated genes (*CD8A*, *GZMB*) in human breast cancer samples from the TCGA dataset.

(D) Frequency of pathologic complete response (pCR) in patients separated by median expression for the indicated genes. Data reflect a cohort of 379 patients constructed from two independent datasets, with significance determined by chi-square.

(E) Recurrence-free survival (RFS) based on median expression of *LAMP3* or *CXCL9* in breast tumor tissue. Data are shown for intrinsic luminal A (n = 1,933), luminal B (n = 1,149), Her2 (n = 251), and basal (n = 618) molecular subtypes. Hazard ratio (HR) and log-rank p values are shown in the upper right of each Kaplan-Meier plot.

See also Figure S7.

interactions to promote T cell effector function. However, whether CXCL9 expression by CD103$^+$ cDC1s is functionally important remains to be shown.

αTIM-3 antibodies have been successfully combined with αPD-1 or αPD-L1 blockade to suppress tumor growth (Ngiow et al., 2011; Sakuishi et al., 2010), and this combination is likely to be the first evaluated clinically. Surprisingly, single-agent efficacy with αTIM-3 has been shown to occur largely independent of CD11c$^+$ cells (Ngiow et al., 2011), whereas our data indicate that cDC1s are necessary mediators of response to combination cytotoxic therapy. This may relate to the restricted expression of IL-12 in CD103$^+$ cDC1s and its critical role in promoting cytotoxic T cell responses within MMTV-PyMT tumors during PTX chemotherapy (Ruffell et al., 2014). As PTX is one of the preferred chemotherapies for use in breast cancer (Rugo et al., 2015), our findings indicate that αTIM-3 antibodies currently in clinical development should also be considered in this setting as a means to improve upon the immune-dependent response to chemotherapy.

STAR★METHODS

Detailed methods are provided in the online version of this paper and include the following:

- KEY RESOURCES TABLE
- CONTACT FOR REAGENT AND RESOURCE SHARING
- EXPERIMENTAL MODEL AND SUBJECT DETAILS
  - Human Studies
  - Animal Studies
- METHOD DETAILS
  - Quantitation of Metastatic Burden
  - Flow Cytometry
  - Gene Expression
  - Immunohistochemistry and Immunofluoresence
  - In Vitro DC Stimulation
  - Transwell Assay
- QUANTIFICATION AND STATISTICAL ANALYSIS

SUPPLEMENTAL INFORMATION

Supplemental Information includes seven figures and can be found with this article online at https://doi.org/10.1016/j.ccell.2017.11.019.

ACKNOWLEDGMENTS

This work was supported by the Moffitt Cancer Center Flow Cytometry, Molecular Genomics, Analytic Microscopy, and Tissue Core Facilities, all comprehensive cancer center facilities designated by the National Cancer Institute (P30-CA076292). The authors would like to thank Vivian Lee, Asmaa El-Kenawi, Jodi Kroeger, Sean Yoder, and Daniel Abate-Daga for technical assistance. Research reported herein was supported by a Breast Cancer Research Foundation grant to H.S.R., Komen Promise award to H.S.R. and L.M.C., DoD Era of Hope Expansion and NCI/NIH grants to L.M.C. (R01CA15531-06, U54CA163123-05), and the Moffitt Cancer Center's Shula Breast Cancer award and NCI/NIH grants (K99CA185325-01A1 and R00CA185325-02) to B.R.

AUTHOR CONTRIBUTIONS

Conceptualization, L.M.C. and B.R.; Investigation, A.d.M.P., A.G., S.H., and B.R.; Resources, M.F.K.; Writing – Original Draft, B.R.; Writing – Review & Editing, A.d.M.P., A.G., H.S., M.F.K., L.M.C., and B.R.; Supervision, B.R.; Funding Acquisition, H.S.R., L.M.C., and B.R.

DECLARATION OF INTERESTS

This work was supported in part by a grant from Tesaro. H.S. has received payments from Novartis International for consulting and advisory boards. B.R. and H.S. have courtesy faculty appointments at the University of South Florida, Tampa.

Received: April 13, 2017
Revised: August 13, 2017
Accepted: November 29, 2017
Published: January 8, 2018

REFERENCES

Alexandrov, L.B., Nik-Zainal, S., Wedge, D.C., Aparicio, S.A., Behjati, S., Biankin, A.V., Bignell, G.R., Bolli, N., Borg, A., Børresen-Dale, A.L., et al. (2013). Signatures of mutational processes in human cancer. Nature *500*, 415–421.

Anderson, A.C., Anderson, D.E., Bregoli, L., Hastings, W.D., Kassam, N., Lei, C., Chandwaskar, R., Karman, J., Su, E.W., Hirashima, M., et al. (2007). Promotion of tissue inflammation by the immune receptor Tim-3 expressed on innate immune cells. Science *318*, 1141–1143.

Anderson, A.C., Joller, N., and Kuchroo, V.K. (2016). Lag-3, Tim-3, and TIGIT: co-inhibitory receptors with specialized functions in immune regulation. Immunity *44*, 989–1004.

Baghdadi, M., Nagao, H., Yoshiyama, H., Akiba, H., Yagita, H., Dosaka-Akita, H., and Jinushi, M. (2013). Combined blockade of TIM-3 and TIM-4 augments cancer vaccine efficacy against established melanomas. Cancer Immunol. Immunother. *62*, 629–637.

Baitsch, L., Baumgaertner, P., Devevre, E., Raghav, S.K., Legat, A., Barba, L., Wieckowski, S., Bouzourene, H., Deplancke, B., Romero, P., et al. (2011). Exhaustion of tumor-specific CD8$^+$ T cells in metastases from melanoma patients. J. Clin. Invest. *121*, 2350–2360.

Bos, P.D., Plitas, G., Rudra, D., Lee, S.Y., and Rudensky, A.Y. (2013). Transient regulatory T cell ablation deters oncogene-driven breast cancer and enhances radiotherapy. J. Exp. Med. *210*, 2435–2466.

Broz, M.L., Binnewies, M., Boldajipour, B., Nelson, A.E., Pollack, J.L., Erle, D.J., Barczak, A., Rosenblum, M.D., Daud, A., Barber, D.L., et al. (2014). Dissecting the tumor myeloid compartment reveals rare activating antigen-presenting cells critical for T cell immunity. Cancer Cell *26*, 638–652.

Cancer Genome Atlas Network. (2012). Comprehensive molecular portraits of human breast tumours. Nature *490*, 61–70.

Chen, D.S., and Mellman, I. (2013). Oncology meets immunology: the cancer-immunity cycle. Immunity *39*, 1–10.

Chiba, S., Baghdadi, M., Akiba, H., Yoshiyama, H., Kinoshita, I., Dosaka-Akita, H., Fujioka, Y., Ohba, Y., Gorman, J.V., Colgan, J.D., et al. (2012). Tumor-infiltrating DCs suppress nucleic acid-mediated innate immune responses through interactions between the receptor TIM-3 and the alarmin HMGB1. Nat. Immunol. *13*, 832–842.

Coffelt, S.B., and de Visser, K.E. (2015). Immune-mediated mechanisms influencing the efficacy of anticancer therapies. Trends Immunol. *36*, 198–216.

DeNardo, D.G., Brennan, D.J., Rexhepaj, E., Ruffell, B., Shiao, S.L., Madden, S.F., Gallagher, W.M., Wadhwani, N., Keil, S.D., Junaid, S.A., et al. (2011). Leukocyte complexity predicts breast cancer survival and functionally regulates response to chemotherapy. Cancer Discov. *1*, 54–67.

Desch, A.N., Randolph, G.J., Murphy, K., Gautier, E.L., Kedl, R.M., Lahoud, M.H., Caminschi, I., Shortman, K., Henson, P.M., and Jakubzick, C.V. (2011). CD103$^+$ pulmonary dendritic cells preferentially acquire and present apoptotic cell-associated antigen. J. Exp. Med. *208*, 1789–1797.

Engelhardt, J.J., Boldajipour, B., Beemiller, P., Pandurangi, P., Sorensen, C., Werb, Z., Egeblad, M., and Krummel, M.F. (2012). Marginating dendritic cells

of the tumor microenvironment cross-present tumor antigens and stably engage tumor-specific T cells. Cancer Cell *21*, 402–417.

Fourcade, J., Sun, Z., Benallaoua, M., Guillaume, P., Luescher, I.F., Sander, C., Kirkwood, J.M., Kuchroo, V., and Zarour, H.M. (2010). Upregulation of Tim-3 and PD-1 expression is associated with tumor antigen-specific $CD8^+$ T cell dysfunction in melanoma patients. J. Exp. Med. *207*, 2175–2186.

Fridman, W.H., Pages, F., Sautes-Fridman, C., and Galon, J. (2012). The immune contexture in human tumours: impact on clinical outcome. Nat. Rev. Cancer *12*, 298–306.

Gorman, J.V., Starbeck-Miller, G., Pham, N.L., Traver, G.L., Rothman, P.B., Harty, J.T., and Colgan, J.D. (2014). Tim-3 directly enhances CD8 T cell responses to acute *Listeria monocytogenes* infection. J. Immunol. *192*, 3133–3142.

Grajales-Reyes, G.E., Iwata, A., Albring, J., Wu, X., Tussiwand, R., Kc, W., Kretzer, N.M., Briseno, C.G., Durai, V., Bagadia, P., et al. (2015). Batf3 maintains autoactivation of Irf8 for commitment of a CD8α(+) conventional DC clonogenic progenitor. Nat. Immunol. *16*, 708–717.

Guy, C.T., Cardiff, R.D., and Muller, W.J. (1992). Induction of mammary tumors by expression of polyomavirus middle T oncogene: a transgenic mouse model for metastatic disease. Mol. Cell Biol *12*, 954–961.

Gyorffy, B., Lanczky, A., Eklund, A.C., Denkert, C., Budczies, J., Li, Q., and Szallasi, Z. (2010). An online survival analysis tool to rapidly assess the effect of 22,277 genes on breast cancer prognosis using microarray data of 1,809 patients. Breast Cancer Res. Treat. *123*, 725–731.

Headley, M.B., Bins, A., Nip, A., Roberts, E.W., Looney, M.R., Gerard, A., and Krummel, M.F. (2016). Visualization of immediate immune responses to pioneer metastatic cells in the lung. Nature *531*, 513–517.

Herbst, R.S., Soria, J.C., Kowanetz, M., Fine, G.D., Hamid, O., Gordon, M.S., Sosman, J.A., McDermott, D.F., Powderly, J.D., Gettinger, S.N., et al. (2014). Predictive correlates of response to the anti-PD-L1 antibody MPDL3280A in cancer patients. Nature *515*, 563–567.

Hess, K.R., Anderson, K., Symmans, W.F., Valero, V., Ibrahim, N., Mejia, J.A., Booser, D., Theriault, R.L., Buzdar, A.U., Dempsey, P.J., et al. (2006). Pharmacogenomic predictor of sensitivity to preoperative chemotherapy with paclitaxel and fluorouracil, doxorubicin, and cyclophosphamide in breast cancer. J. Clin. Oncol. *24*, 4236–4244.

Hildner, K., Edelson, B.T., Purtha, W.E., Diamond, M., Matsushita, H., Kohyama, M., Calderon, B., Schraml, B.U., Unanue, E.R., Diamond, M.S., et al. (2008). Batf3 deficiency reveals a critical role for $CD8alpha^+$ dendritic cells in cytotoxic T cell immunity. Science *322*, 1097–1100.

Iijima, N., and Iwasaki, A. (2014). T cell memory. A local macrophage chemokine network sustains protective tissue-resident memory CD4 T cells. Science *346*, 93–98.

Jackson, J.T., Hu, Y., Liu, R., Masson, F., D'Amico, A., Carotta, S., Xin, A., Camilleri, M.J., Mount, A.M., Kallies, A., et al. (2011). Id2 expression delineates differential checkpoints in the genetic program of $CD8\alpha^+$ and $CD103^+$ dendritic cell lineages. EMBO J. *30*, 2690–2704.

Jin, H.T., Anderson, A.C., Tan, W.G., West, E.E., Ha, S.J., Araki, K., Freeman, G.J., Kuchroo, V.K., and Ahmed, R. (2010). Cooperation of Tim-3 and PD-1 in CD8 T-cell exhaustion during chronic viral infection. Proc. Natl. Acad. Sci. USA *107*, 14733–14738.

Jones, R.B., Ndhlovu, L.C., Barbour, J.D., Sheth, P.M., Jha, A.R., Long, B.R., Wong, J.C., Satkunarajah, M., Schweneker, M., Chapman, J.M., et al. (2008). Tim-3 expression defines a novel population of dysfunctional T cells with highly elevated frequencies in progressive HIV-1 infection. J. Exp. Med. *205*, 2763–2779.

Kane, L.P. (2010). T cell Ig and mucin domain proteins and immunity. J. Immunol. *184*, 2743–2749.

Kanzaki, M., Wada, J., Sugiyama, K., Nakatsuka, A., Teshigawara, S., Murakami, K., Inoue, K., Terami, T., Katayama, A., Eguchi, J., et al. (2012). Galectin-9 and T cell immunoglobulin mucin-3 pathway is a therapeutic target for type 1 diabetes. Endocrinology *153*, 612–620.

Kastenmuller, W., Brandes, M., Wang, Z., Herz, J., Egen, J.G., and Germain, R.N. (2013). Peripheral prepositioning and local CXCL9 chemokine-mediated guidance orchestrate rapid memory $CD8^+$ T cell responses in the lymph node. Immunity *38*, 502–513.

Katoh, S., Ishii, N., Nobumoto, A., Takeshita, K., Dai, S.Y., Shinonaga, R., Niki, T., Nishi, N., Tominaga, A., Yamauchi, A., and Hirashima, M. (2007). Galectin-9 inhibits CD44-hyaluronan interaction and suppresses a murine model of allergic asthma. Am. J. Respir. Crit. Care Med. *176*, 27–35.

Kroemer, G., Galluzzi, L., Kepp, O., and Zitvogel, L. (2013). Immunogenic cell death in cancer therapy. Annu. Rev. Immunol. *31*, 51–72.

Le, D.T., Uram, J.N., Wang, H., Bartlett, B.R., Kemberling, H., Eyring, A.D., Skora, A.D., Luber, B.S., Azad, N.S., Laheru, D., et al. (2015). PD-1 blockade in tumors with mismatch-repair deficiency. N. Engl. J. Med. *372*, 2509–2520.

Lee, J., Su, E.W., Zhu, C., Hainline, S., Phuah, J., Moroco, J.A., Smithgall, T.E., Kuchroo, V.K., and Kane, L.P. (2011). Phosphotyrosine-dependent coupling of Tim-3 to T-cell receptor signaling pathways. Mol. Cell Biol *31*, 3963–3974.

Leitner, J., Rieger, A., Pickl, W.F., Zlabinger, G., Grabmeier-Pfistershammer, K., and Steinberger, P. (2013). TIM-3 does not act as a receptor for galectin-9. PLoS Pathog. *9*, e1003253.

Maroulakou, I.G., Anver, M., Garrett, L., and Green, J.E. (1994). Prostate and mammary adenocarcinoma in transgenic mice carrying a rat C3(1) simian virus 40 large tumor antigen fusion gene. Proc. Natl. Acad. Sci. USA *91*, 11236–11240.

Maurya, N., Gujar, R., Gupta, M., Yadav, V., Verma, S., and Sen, P. (2014). Immunoregulation of dendritic cells by the receptor T cell Ig and mucin protein-3 via Bruton's tyrosine kinase and c-Src. J. Immunol. *193*, 3417–3425.

Monney, L., Sabatos, C.A., Gaglia, J.L., Ryu, A., Waldner, H., Chernova, T., Manning, S., Greenfield, E.A., Coyle, A.J., Sobel, R.A., et al. (2002). Th1-specific cell surface protein Tim-3 regulates macrophage activation and severity of an autoimmune disease. Nature *415*, 536–541.

Nakayama, M., Akiba, H., Takeda, K., Kojima, Y., Hashiguchi, M., Azuma, M., Yagita, H., and Okumura, K. (2009). Tim-3 mediates phagocytosis of apoptotic cells and cross-presentation. Blood *113*, 3821–3830.

Natsuaki, Y., Egawa, G., Nakamizo, S., Ono, S., Hanakawa, S., Okada, T., Kusuba, N., Otsuka, A., Kitoh, A., Honda, T., et al. (2014). Perivascular leukocyte clusters are essential for efficient activation of effector T cells in the skin. Nat. Immunol. *15*, 1064–1069.

Ngiow, S.F., von Scheidt, B., Akiba, H., Yagita, H., Teng, M.W., and Smyth, M.J. (2011). Anti-TIM3 antibody promotes T cell IFN-γ-mediated antitumor immunity and suppresses established tumors. Cancer Res. *71*, 3540–3551.

Oikawa, T., Kamimura, Y., Akiba, H., Yagita, H., Okumura, K., Takahashi, H., Zeniya, M., Tajiri, H., and Azuma, M. (2006). Preferential involvement of Tim-3 in the regulation of hepatic $CD8^+$ T cells in murine acute graft-versus-host disease. J. Immunol. *177*, 4281–4287.

Phong, B.L., Avery, L., Sumpter, T.L., Gorman, J.V., Watkins, S.C., Colgan, J.D., and Kane, L.P. (2015). Tim-3 enhances FcepsilonRI-proximal signaling to modulate mast cell activation. J. Exp. Med. *212*, 2289–2304.

Rangachari, M., Zhu, C., Sakuishi, K., Xiao, S., Karman, J., Chen, A., Angin, M., Wakeham, A., Greenfield, E.A., Sobel, R.A., et al. (2012). Bat3 promotes T cell responses and autoimmunity by repressing Tim-3–mediated cell death and exhaustion. Nat. Med. *18*, 1394–1400.

Rizvi, N.A., Hellmann, M.D., Snyder, A., Kvistborg, P., Makarov, V., Havel, J.J., Lee, W., Yuan, J., Wong, P., Ho, T.S., et al. (2015). Cancer immunology. Mutational landscape determines sensitivity to PD-1 blockade in non-small cell lung cancer. Science *348*, 124–128.

Roberts, E.W., Broz, M.L., Binnewies, M., Headley, M.B., Nelson, A.E., Wolf, D.M., Kaisho, T., Bogunovic, D., Bhardwaj, N., and Krummel, M.F. (2016). Critical role for CD103(+)/CD141(+) dendritic cells bearing CCR7 for tumor antigen trafficking and priming of T cell immunity in melanoma. Cancer Cell *30*, 324–336.

Ruffell, B., Au, A., Rugo, H.S., Esserman, L.J., Hwang, E.S., and Coussens, L.M. (2012). Leukocyte composition of human breast cancer. Proc. Natl. Acad. Sci. USA *109*, 2796–2801.

Ruffell, B., Chang-Strachan, D., Chan, V., Rosenbusch, A., Ho, C.M., Pryer, N., Daniel, D., Hwang, E.S., Rugo, H.S., and Coussens, L.M. (2014). Macrophage

IL-10 blocks CD8$^+$ T cell-dependent responses to chemotherapy by suppressing IL-12 expression in intratumoral dendritic cells. Cancer Cell *26*, 623–637.

Rugo, H.S., Barry, W.T., Moreno-Aspitia, A., Lyss, A.P., Cirrincione, C., Leung, E., Mayer, E.L., Naughton, M., Toppmeyer, D., Carey, L.A., et al. (2015). Randomized phase III trial of paclitaxel once per week compared with nanoparticle albumin-bound nab-paclitaxel once per week or ixabepilone with bevacizumab as first-line chemotherapy for locally recurrent or metastatic breast cancer: CALGB 40502/NCCTG N063H (alliance). J. Clin. Oncol. *33*, 2361–2369.

Sakuishi, K., Apetoh, L., Sullivan, J.M., Blazar, B.R., Kuchroo, V.K., and Anderson, A.C. (2010). Targeting Tim-3 and PD-1 pathways to reverse T cell exhaustion and restore anti-tumor immunity. J. Exp. Med. *207*, 2187–2194.

Salgado, R., Denkert, C., Demaria, S., Sirtaine, N., Klauschen, F., Pruneri, G., Wienert, S., Van den Eynden, G., Baehner, F.L., Penault-Llorca, F., et al. (2015). The evaluation of tumor-infiltrating lymphocytes (TILs) in breast cancer: recommendations by an International TILs Working Group 2014. Ann. Oncol. *26*, 259–271.

Salmon, H., Idoyaga, J., Rahman, A., Leboeuf, M., Remark, R., Jordan, S., Casanova-Acebes, M., Khudoynazarova, M., Agudo, J., Tung, N., et al. (2016). Expansion and activation of CD103(+) dendritic cell progenitors at the tumor site enhances tumor responses to therapeutic PD-L1 and BRAF inhibition. Immunity *44*, 924–938.

Sanchez-Paulete, A.R., Cueto, F.J., Martinez-Lopez, M., Labiano, S., Morales-Kastresana, A., Rodriguez-Ruiz, M.E., Jure-Kunkel, M., Azpilikueta, A., Aznar, M.A., Quetglas, J.I., et al. (2015). Cancer immunotherapy with immunomodulatory anti-CD137 and anti-PD-1 Monoclonal antibodies requires BATF3-dependent dendritic cells. Cancer Discov. *6*, 71–79.

Seillet, C., Jackson, J.T., Markey, K.A., Brady, H.J., Hill, G.R., Macdonald, K.P., Nutt, S.L., and Belz, G.T. (2013). CD8α^+ DCs can be induced in the absence of transcription factors Id2, Nfil3, and Batf3. Blood *121*, 1574–1583.

Sistigu, A., Yamazaki, T., Vacchelli, E., Chaba, K., Enot, D.P., Adam, J., Vitale, I., Goubar, A., Baracco, E.E., Remedios, C., et al. (2014). Cancer cell-autonomous contribution of type I interferon signaling to the efficacy of chemotherapy. Nat. Med. *20*, 1301–1309.

Spranger, S., Bao, R., and Gajewski, T.F. (2015). Melanoma-intrinsic beta-catenin signalling prevents anti-tumour immunity. Nature *523*, 231–235.

Spranger, S., Dai, D., Horton, B., and Gajewski, T.F. (2017). Tumor-residing Batf3 dendritic cells are required for effector T cell trafficking and adoptive T cell therapy. Cancer Cell *31*, 711–723.e4.

Su, E.W., Bi, S., and Kane, L.P. (2011). Galectin-9 regulates T helper cell function independently of Tim-3. Glycobiology *21*, 1258–1265.

Tabchy, A., Valero, V., Vidaurre, T., Lluch, A., Gomez, H., Martin, M., Qi, Y., Barajas-Figueroa, L.J., Souchon, E., Coutant, C., et al. (2010). Evaluation of a 30-gene paclitaxel, fluorouracil, doxorubicin, and cyclophosphamide chemotherapy response predictor in a multicenter randomized trial in breast cancer. Clin. Cancer Res. *16*, 5351–5361.

Tumeh, P.C., Harview, C.L., Yearley, J.H., Shintaku, I.P., Taylor, E.J., Robert, L., Chmielowski, B., Spasic, M., Henry, G., Ciobanu, V., et al. (2014). PD-1 blockade induces responses by inhibiting adaptive immune resistance. Nature *515*, 568–571.

Walser, T.C., Rifat, S., Ma, X., Kundu, N., Ward, C., Goloubeva, O., Johnson, M.G., Medina, J.C., Collins, T.L., and Fulton, A.M. (2006). Antagonism of CXCR3 inhibits lung metastasis in a murine model of metastatic breast cancer. Cancer Res. *66*, 7701–7707.

Van Allen, E.M., Miao, D., Schilling, B., Shukla, S.A., Blank, C., Zimmer, L., Sucker, A., Hillen, U., Foppen, M.H., Goldinger, S.M., et al. (2015). Genomic correlates of response to CTLA-4 blockade in metastatic melanoma. Science *350*, 207–211.

van de Weyer, P.S., Muehlfeit, M., Klose, C., Bonventre, J.V., Walz, G., and Kuehn, E.W. (2006). A highly conserved tyrosine of Tim-3 is phosphorylated upon stimulation by its ligand galectin-9. Biochem. Biophys. Res. Commun. *351*, 571–576.

Yadav, M., Jhunjhunwala, S., Phung, Q.T., Lupardus, P., Tanguay, J., Bumbaca, S., Franci, C., Cheung, T.K., Fritsche, J., Weinschenk, T., et al. (2014). Predicting immunogenic tumour mutations by combining mass spectrometry and exome sequencing. Nature *515*, 572–576.

Zhu, C., Anderson, A.C., Schubart, A., Xiong, H., Imitola, J., Khoury, S.J., Zheng, X.X., Strom, T.B., and Kuchroo, V.K. (2005). The Tim-3 ligand galectin-9 negatively regulates T helper type 1 immunity. Nat. Immunol. *6*, 1245–1252.

STAR★METHODS

KEY RESOURCES TABLE

REAGENT or RESOURCE	SOURCE	IDENTIFIER
Antibodies		
Anti-mouse Ly6G clone 1A8 BUV395	BD	Cat# 563978; RRID: AB_2716852
Anti-mouse CD24 clone M1/69 BUV496	BD	Cat# 564664; RRID: AB_2716853
Anti-mouse CD19 clone 1D3 BUV737	BD	Cat# 564296; RRID: AB_2716855
Anti-mouse CD8 alpha clone 53.6-7 BUV800	BD	Cat# 564920; RRID: AB_2716856
Anti-mouse MHCII M5/114.15.2 BV421	BD	Cat# 562564; RRID: AB_2716857
Anti-mouse gamma delta TCR clone GL3 BV510	BD	Cat# 563218; RRID: AB_2716858
Anti-mouse CD11c clone N418 BV605	BioLegend	Cat# 117334; RRID: AB_2562415
Anti-mouse CD4 clone RM4-5 BV650	BD	Cat# 563747; RRID: AB_2716859
Anti-mouse/human CD11b M1/70 BV711	BD	Cat# 563168; RRID: AB_2716860
Anti-mouse CD45 30-F11 BV786	BD	Cat# 564225; RRID: AB_2716861
Anti-mouse CD69 H1/2F3 FITC	BioLegend	Cat# 104506; RRID: AB_313109
Anti-mouse CD3 epsilon clone 17A2 PerCP-Cy5.5	BD	Cat# 560527; RRID: AB_1727463
Anti-mouse PDCA-1 clone 927 PE	BioLegend	Cat# 127010; RRID: AB_1953285
Anti-mouse CD49b clone DX5 PE-Dazzle	BioLegend	Cat# 108924; RRID: AB_2565271
Anti-mouse CD103 clone 2E7 PE-Cy7	BioLegend	Cat #121426; RRID: AB_2563691
Anti-mouse F4/80 clone BM8 APC	BioLegend	Cat# 123116; RRID: AB_893481
Anti-mouse Ly6C clone HK1.4 APC-Cy7	BioLegend	Cat# 128026; RRID: AB_10640120
Anti-mouse IL-12p40 clone C15.6 PE	BioLegend	Cat# 505204; RRID: AB_315368
Anti-mouse/human granzyme B clone GB11 Alexa647	BioLegend	Cat# 515406; RRID: AB_2566333
Anti-mouse CXCL9 PE	BioLegend	Cat# 515604; RRID: AB_2245489
Anti-mouse IFN gamma clone XMG1.2 PE-Cy7	BioLegend	Cat# 505826; RRID: AB_2295770
Anti-mouse TNF alpha clone MP6-XT22 PE	BioLegend	Cat# 506306; RRID: AB_315427
Anti-mouse TIM-3 clone RMT3-23 PE	BioLegend	Cat# 119703; RRID: AB_345377
Anti-mouse CD16/CD32 clone 2.4G2 (Fc block)	BD	Cat# 553142; RRID: AB_394657
Anti-mouse CD3 epsilon clone 145-2C11 biotin	BioLegend	Cat# 100304; RRID: AB_312669
Anti-mouse/human B220 clone RA3-6B2 biotin	BioLegend	Cat# 103204; RRID: AB_312989
Anti-mouse Ly6G clone 1A8 biotin	BioLegend	Cat# 127604; RRID: AB_1186108
Anti-mouse CD49b clone DX5 biotin	BioLegend	Cat# 108904; RRID: AB_313411
Anti-mouse Ter119 clone TER-119 biotin	BioLegend	Cat# 116204; RRID: AB_313705
Anti-mouse TIM-3 clone RMT3-23 (LEAF)	BioLegend	Cat# 119708; RRID: AB_2564109
Anti-mouse/human HMGB1 clone 3E8	BioLegend	Cat# 651401; RRID: AB_10945159
Anti-mouse CEACAM-1 clone MAb-CC1 (LEAF)	BioLegend	Cat# 134504; RRID: AB_1659209
Anti-mouse TIM-3 clone RMT3-23	BioXCell	Cat# BE0115; RRID: AB_10949464
Anti-mouse Galectin-9 clone RG9-1	BioXCell	Cat# BE0218; RRID: AB_2687702
Anti-mouse TIM-4 clone RMT4-53	BioXCell	Cat# BE0171; RRID: AB_2687695
Anti-mouse CD8 alpha clone 2.43	BioXCell	Cat# BE0061; RRID: AB_1125541
Anti-mouse CD8 beta clone 53-5.8	BioXCell	Cat# BE0223; RRID: AB_2687706
Anti-mouse IL-12p75 clone R2-9A5	BioXCell	Cat# BE0233; RRID: AB_2687715
Anti-mouse IFN gamma clone XMG1.2	BioXCell	Cat# BE0055; RRID: AB_1107694
Anti-mouse IFNAR1 clone MAR1-5A3	BioXCell	Cat# BE0241; RRID: AB_2687723
Anti-mouse PD-1 clone RMP1-14	BioXCell	Cat# BE0146; RRID: AB_10949053
Anti-mouse CXCR3 clone CXCR3-173	BioXCell	Cat# BE0249; RRID: AB_2687730
Rat anti-HRPN Isotype Control (IgG1)	BioXCell	Cat# BE0088; RRID: AB_1107775
Rat anti trinitrophenol Isotype Control (IgG2a)	BioXCell	Cat# BE0089; RRID: AB_1107769

(*Continued on next page*)

Continued

REAGENT or RESOURCE	SOURCE	IDENTIFIER
Anti-mouse Ki67 clone D3B5	Cell Signaling	Cat# 12202; RRID: AB_2620142
Anti-mouse/human cleaved caspase 3 (Rabbit polyclonal)	Cell Signaling	Cat# 9661; RRID: AB_2341188
Anti-human TIM-3 clone D5D5R	Cell Signaling	Cat# 45208; RRID: AB_2716862
Anti-human Galectin-9 clone 1D12	Novus Biologicals	Cat# NBP2-45619; RRID: AB_2716863
Anti-human DC-LAMP (goat polyclonal)	R&D Systems	Cat# AF4087; RRID: AB_2134868
Anti-human/mouse pan-keratin clone C11	Cell Signaling	Cat# 4545; RRID: AB_490860
Anti-human CD45 clone PD7/26/16+2B11	ThermoFisher	Cat# MA5-13197; RRID: AB_11001172
Anti-human CD3 epsilon clone PS1	ThermoFisher	Cat# MS401S0; RRID: AB_61226
Anti-human CD8 alpha clone C8/144B	ThermoFisher	Cat# MS457S0; RRID: AB_61028
Anti-human CD4 clone 4B12	ThermoFisher	Cat# MS1528S0; RRID: AB_62559
Anti-human CD163 clone 10D6	ThermoFisher	Cat# MS1103S0; RRID: AB_64139
Anti-human CXCL9 rabbit polyclonal	ThermoFisher	Cat# PA5-34743; RRID: AB_2552095
Anti-human CD45 clone H130 BV785	BD	Cat# 563716; RRID: AB_2716864
Anti-human HLA-DR clone L243 APC-Fire750	BioLegend	Cat# 307658; RRID: AB_2572101
Anti-human CD16 clone 3G8 BV421	BD	Cat# 562874; RRID: AB_2716865
Anti-human CCR7 clone G043H7 BV711	BioLegend	Cat# 353228; RRID: AB_2563865
Anti-human TIM-3 clone F38-2E2 PE	BD	Cat# 563422; RRID: AB_2716866
Anti-human CD3 epsilon clone OKT3 PerCP710	eBioscience	Cat# 46-0037-42; RRID: AB_1834395
Anti-human CD56 clone HCD56 PE-Cy7	BioLegend	Cat# 318318; RRID: AB_604107
Anti-human CD19 clone SJ25C1 BUV737	BD	Cat# 564303; RRID: AB_2716867
Anti-human CD4 clone RPA-T4 BV605	BioLegend	Cat# 300556; RRID: AB_2564391
Anti-human CD11c clone 3.9 BV650	BioLegend	Cat# 301638; RRID: AB_2563797
Anti-human CD14 clone M5E2 BUV805	BD	Cat# 565779; RRID: AB_2716868
Anti-human CD11b clone ICRF44 BUV395	BD	Cat# 563839; RRID: AB_2716869
Anti-human BDCA1/CD1c clone F10/21A3 BB515	BD	Cat# 565054; RRID: AB_2716870
Anti-human BDCA3/CD141 clone M80 APC	BioLegend	Cat# 344106; RRID: AB_10899578
Anti-human CD123 clone 6H6 PE-Dazzle	BioLegend	Cat# 306034; RRID: AB_2566450
Anti-human CD117 clone YB5.B8 APC-R700	BD	Cat# 565195; RRID: AB_2716871
Biological Samples		
Adult breast tumor tissue	Moffitt Cancer Center Tissue Core Facility	N/A
Adult peripheral blood mononuclear cells	OneBlood	N/A
Chemicals, Peptides, and Recombinant Proteins		
Paclitaxel	Mylan or Hospira	
Carboplatin	Teva Pharmaceutical	
Human Flt-3L-Ig	BioXCell	Cat# BE0098; RRID: AB_10949072
Recombinant mouse IFN-γ	Peprotech	315-05
Recombinant mouse IL-10	Peprotech	210-10
Recombinant mouse VEGF-A	Peprotech	450-32
Recombinant mouse CXCL9 (MIG)	BioLegend	578204
Recombinant mouse CXCL10 (IP-10)	BioLegend	573604
Poly(I:C) LMW	InvivoGen	tlrl-picw
LPS-EB Ultrapure	InvivoGen	tlrl-3pelps
Imiquimod	InvivoGen	tlrl-imqs
CpG ODN2395	InvivoGen	tlrl-2395
Brefeldin A	Sigma-Aldrich	B6542
Brefeldin A (1000x solution)	BioLegend	420601
FTY720	Sigma-Aldrich	SML0700

(*Continued on next page*)

Continued

REAGENT or RESOURCE	SOURCE	IDENTIFIER
(±)-AMG 487	R&D Systems	4487/10
Cell Activation Cocktail	BioLegend	423303
Diphtheria Toxin	Sigma-Aldrich	D0564
Matrigel GFR/LDEV-Free	Fisher Scientific	CB-40230
Live/Dead Fixable Aqua Dead Cell Stain	ThermoFisher Scientific	L34957
Zombie NIR Fixable Viability Kit	BioLegend	423105
TrueStain FcX Block	BioLegend	422302
Critical Commercial Assays		
Single Tube TaqMan Gene Expression Assays	ThermoFisher Scientific	4331182
nCounter Mouse Immunology Panel	NanoString	XT-CSO-MIM1-12
ImmPRESS HRP Anti-Mouse Ig	Vector Labs	Cat# MP-7402; RRID: AB_2336528
ImmPRESS HRP Anti-Rabbit Ig	Vector Labs	Cat# MP-7401; RRID: AB_2336529
ImmPRESS HRP Anti-Goat Ig	Vector Labs	Cat# MP-7405; RRID: AB_2336526
Deposited Data		
Gene array of FNAs prior to chemotherapy	Hess et al., 2006	GSE20194
Gene array of FNAs prior to chemotherapy	Tabchy et al., 2010	GSE20271
TCGA Breast Cancer dataset	Cancer Genome Atlas Network, 2012	https://cancergenome.nih.gov/
Experimental Models: Organisms/Strains		
Mouse: FVB/N-Tg(MMTV-PyVT)634Mul/J	Guy et al., 1992	JAX: 002374; RRID: IMSR_JAX:002374
Mouse: B6.FVB-Tg(MMTV-PyVT)634Mul/J	The Jackson Laboratory	JAX: 022974; RRID: IMSR_JAX:022974
Mouse: PyMTchOVA; backcrossed to FVB/NJ x10	Engelhardt et al., 2012	N/A
Mouse: B6.129S9C)-Batf3tm1Kmm/J; backcrossed to FVBN/J x5	Hildner et al., 2008	JAX: 013755; RRID: IMSR_JAX:013755
Mouse: FVB-Tg(C3-1-TAg)cJeg/JegJ	Maroulakou et al., 1994	JAX: 013591; RRID: IMSR_JAX:013591
Mouse: B6.Cg-Tg(Itgax-cre)1-1Reiz/J	The Jackson Laboratory	JAX: 008068; RRID: IMSR_JAX:008068
Mouse: BC(Cg)-Irf8tm1.1hm/J	The Jackson Laboratory	JAX: 014175; RRID: IMSR_JAX:014175
Mouse: B6(Cg)-*Zbtb46*$^{tm1(HBEGF)Mnz}$/J	The Jackson Laboratory	JAX: 019506; RRID: IMSR_JAX:019506
Mouse: FVB/NJ	The Jackson Laboratory	JAX: 001800; RRID: IMSR_JAX:001800
Mouse: C57BL/6J	The Jackson Laboratory	JAX: 000664; RRID: IMSR_JAX:000664
Software and Algorithms		
FlowJo Version 9 and 10	FlowJo LLC	https://www.flowjo.com/
Prism Version 6 and 7	GraphPad	https://www.graphpad.com/scientific-software/prism/
Kaplan-Meier Plotter	Gyorffy et al., 2010	http://kmplot.com/analysis/
GENE-E	Broad Institute	http://www.broadinstitute.org/cancer/software/GENE-E/

CONTACT FOR REAGENT AND RESOURCE SHARING

Further information and requests for resources and reagents should be directed to and will be fulfilled by the Lead Contact, Brian Ruffell (Brian.Ruffell@moffitt.org).

EXPERIMENTAL MODEL AND SUBJECT DETAILS

Human Studies

Human biospecimens were consented and collected through Moffitt Cancer Center''s Total Cancer Care general banking protocol (MCC#14690/Chesapeake IRB approval #Pro00014441). De-identified formalin-fixed paraffin embedded breast tissues were released in support of this study with an SRC and IRB approved protocol (MCC#50168/Chesapeake IRB Pro00019964). Breast tumors for flow cytometry were obtained from adult female patients under Chesapeake IRB approval #Pro00050168. De-identified

peripheral blood mononuclear cells of unknown gender were purchased from OneBlood. Patient consent forms for all samples were obtained at the time of tissue acquisition.

Animal Studies

Animals were maintained in either the Oregon Health & Science University or University of South Florida Department of Comparative Medicine barrier facility, and the respective Institutional Animal Care and Use Committee approved all experiments. Female FVB/NJ strain background mice harboring the polyoma middle T (PyMT) transgene under the control of the mouse mammary tumor virus (MMTV) promoter (Guy et al., 1992), and the simian virus 40 large tumor antigen (SV40 TAg) under control of the rat prostatic steroid binding protein gene [C3(1)] (Maroulakou et al., 1994) have been previously described. PyMTchOVA mice expressing PyMT, mCherry, and ovalbumin under control of the MMTV promoter (Engelhardt et al., 2012) were backcrossed onto FVB/NJ mice 10 generations. *Batf3*-deficient mice (Hildner et al., 2008) were a kind gift of Kenneth Murphy (Washington University School of Medicine, St. Louis) and were backcrossed onto FVB/NJ mice 5 generations. *Itgax-cre*, *Irf8*$^{fl/fl}$, *Zbtb46-DTR*, and MMTV-PyMT mice on the C57BL/6J background mice were acquired from The Jackson Laboratory. Bone marrow chimeric mice were generated by irradiating recipient mice with 2 doses of 500 rads, followed by a bone marrow transfer from donor animals, with tumors implanted after an additional 6 weeks. Implantation of orthotopic mammary tumors was performed in female mice (approximately 2–-4 months of age) by using single-cell suspensions isolated from mammary tumors of MMTV-PyMT transgenic mice combined 1:1 with matrigel (Corning), and injecting 10^6 cells/100 μl into the right 2/3 mammary gland. For MMTV-PyMT animals treatment schedules were initiated in non-blinded fashion with age-matched littermates (day 80-85) randomized to treatment groups as indicated in the respective figures. C3(1)-TAg animals were treated when tumors reached 1 cm in diameter (approximately 5-8 months of age). Monoclonal antibodies (IgG_1/HRPN, IgG_{2a}/2A3, αTIM-3/RMT3-23, αTIM-4/RMT4-53, αCD8α/2.43, αCD8β/53-5.8, αIL-12p75/R2-9A5, αIFN-γ/XMG1.2, αIFNAR1/MAR1-5A3, αGalectin-9/RG9-1, αPD-1/RMP1-14, αCXCR3/CXCR3-173) were obtained from BioXCell and were administered by intraperitoneal (i.p.) injection at 1.0 mg/mouse, with follow-up doses of 0.5 mg every 5 days. FTY720 from Sigma-Aldrich was administered i.p. every 2 days at 20 μg per animal. DT (Sigma-Aldrich) was injected i.p. at 20 ng/g to start, and then at 4 ng/g every 2nd day. (±)-AMG 487 from R&D Systems was dissolved in 20% (2-hydroxypropyl)-β-cyclodextrin (Sigma-Aldrich) and was administered i.p twice daily at 5 μg/g as described (Walser et al., 2006). Clinical grade PTX (Hospira or Mylan) or carboplatin (Teva Pharmaceutical) was administered intravenously every 5 days at 10 mg/kg or 20 mg/kg, respectively.

METHOD DETAILS

Quantitation of Metastatic Burden

Following resection, lungs from transgenic MMTV-PyMT animals were injected with neutral buffered formalin via the trachea and incubated overnight in formalin prior to ethanol dehydration and paraffin embedding. Five lungs sections, each 100 μm apart, were haematoxylin and eosin stained and digitally scanned with an Aperio ScanScope CS Slide Scanner. Frequency and size of the metastatic foci were determined by manual circling in a blinded fashion using Imagescope software (Aperio).

Flow Cytometry

Mice were cardiac-perfused with PBS containing 10 U/ml heparin to clear peripheral blood, and single cell suspensions were prepared by incubating minced tissue in 1 mg/ml collagenase (Roche) and 50 U/ml DNase I (Roche) at 35°C with agitation. Cells were used immediately or stored in 10% DMSO at -80°C. Immune populations were identified with a previously described gating strategy (Ruffell et al., 2014) using antibodies described in the Key Resources Table. Ex vivo intracellular staining for IL-12p40 (clone C15.6), granyzme B (clone GB11), or CXCL9 (clone MIG-2F5.5) was performed on isolated cells 4-6 hr following an intravenous injection of 0.25 mg brefeldin A (Sigma-Aldrich). Alternatively, a single cell suspension was stimulated for 4 hr in vitro with Cell Activation Cocktail with Brefeldin A (BioLegend) or IFN-γ (40 ng/ml) in the presence of 5 μg/ml brefeldin A (BioLegend), and then stained for intracellular CXCL9, IFN-γ (clone XMG1.2), or TNF-α (clone MP6-XT22). Data was collected with either an LSRII or Fortessa flow cytometer (BD Bioscience). Human breast tumors were prepared as described above using antibodies listed in the Key Resources Table and the gating strategy shown in Figure S1 (Ruffell et al., 2012), with data collected using a BD FACSymphony. All analysis was performed using FlowJo version 9 or 10 (FlowJo LLC).

Gene Expression

Fluorescent-activated cell sorting (FACS) was conducted on a FACSAriaII (BD Biosciences), with 2,000 to 50,000 sorted cells flash frozen in liquid nitrogen as a cell pellet. For real-time PCR analysis RNA was prepared using RNeasy Micro kit guidelines (Qiagen). Contaminating DNA was removed with DNAse I (Life Technologies), and then SuperScript III (Life Technologies) was used to reverse transcribe purified RNA into cDNA according to manufacturer's directions. PCR was performed using individual TaqMan Assays following a preamplification step (Life Technologies). The comparative threshold cycle method was used to calculate fold change in gene expression, which was normalized to a single (*Tbp*) reference gene. For gene expression analysis by Nanostring nCounter, cell lysates were hybridized to the 561 gene Mouse Immunology Panel according to the manufacturer's protocol (NanoString Technologies). Briefly, 10 μl of Ambion Cells-to-Ct buffer (Thermo Fisher Scientific) was added to a cell pellet and a 5.0 μl volume of lysate

was hybridized to the NanoString reporter and capture probes in a thermal cycler for 16 hr at 65°C. Washing and cartridge immobilization were performed on the NanoString nCounter PrepStation, and the cartridge was scanned at 555 fields of view on the nCounter Digital Analyzer. The resulting RCC files containing raw counts were reviewed for quality and normalized in the NanoString nSolver Analysis Software v2.5, followed by exportation and analysis.

Immunohistochemistry and Immunofluoresence

5 μm sections of formalin fixed, paraffin embedded tissue were deparaffinized with xylene, rehydrated, and subjected to antigen retrieval with heated antigen unmasking solution (1.0 mM EDTA, 0.05% Tween 20, pH 8.0). After 1 hr in horse serum blocking buffer, primary antibodies were applied for 3 hr at room temperature or overnight at 4°C. Anti-human antibodies included TIM-3 (1:100 for IF, 1:400 for IHC, Clone D5D5R, Cell Signaling), Galectin-9 (1:100, Clone 1D12, Novus Biologicals), DC-LAMP (1:100, #AF4087, R&D Systems), pan-cytokeratin Alexa 488 (1:100, Clone C11, Cell Signaling); and the following from Thermo Scientific: CD45 (1:100, Clone PD7/26/16+2B11), CD3ε (1:100, Clone PS1), CD8 (1:50, Clone C8/144B), CD4 (1:50, Clone 4B12), CD163 (1:50, Clone 10D6), CXCL9 (1:100, Rabbit Polyclonal). Anti-mouse antibodies included cleaved caspase 3 (1:200, Cell Signaling #9661) and Ki67 (1:400, Clone D3B5, Cell Signaling). For immunohistochemistry, the ImmPRESS detection system was used with DAB chromogen, followed by counterstaining with hematoxylin QS (all from Vector Labs). Slides were digitally scanned using the Aperio ScanScope CS Slide Scanner with a 40X objective, and automated quantitative image analysis was performed using Imagescope and the nuclear detection algorithm (Leica Biosystems). For immunofluorescence, secondary antibodies were used at 1:500 for 1 hr at room temperature, followed by incubation with 1.0 μg/ml Hoechst 33342 for 15 min (all from Invitrogen). Slides were then washed and mounted with ProLong Gold anti-fade mounting medium (Invitrogen), and images were acquired with a Zeiss Axio Imager Z1.

In Vitro DC Stimulation

Bone marrow was harvested from FVB/NJ female mice and red blood cells lysed with 150 mM NH_4Cl/10 mM $NaHCO_3$/1 mM EDTA. Remaining cells were plated at $2x10^6$ per ml in RPMI 1640 containing 2.0 mM L-glutamine and 25 mM HEPES, supplemented with 10 mM Sodium Pyruvate, nonessential amino acids, 100 U/ml penicillin/streptomycin, 55 μM β-ME, and 10% fetal calf serum (Life Technologies). Recombinant human Flt-3 Ligand Immunoglobulin (Flt-3L-Ig; BioXCell) was added at 100 ng/ml and cells were incubated untouched for 7 days. Cells in suspension were removed by pipetting (>90% $CD11c^+$), resuspended at 10^6 per ml in RPMI1640 with 100 ng/ml Flt-3L-Ig, and incubated for 24 hr with the following reagents: IFN-γ (40 ng/ml; Peprotech), αCD40 (10 μg/ml; FGK4.5; BioXCell), Poly(I:C)-LMW, LPS-EB Ultrapure, Imiquimod, or CpG ODN2395 (all at 1 μg/ml; InvivoGen), IL-10 (1-100 U/ml; Peprotech), and/or VEGFA (1-100 U/ml; Peprotech).

Splenic cDC were enriched (~50% purity) by negative selection using biotinylated antibodies against CD3, B220, Ly6G, CD49b and Ter119 in combination with MojoSort magnetic beads (BioLegend). Cells were plated at $1x10^6$ per ml in serum free RPMI 1640 and stimulated for 6 hr with the agents described above in the presence of 5 μg/ml brefeldin A (BioLegend), or suspended in supernatant containing tumor cell debris created by irradiation (15,000 Rads, harvest after 48 hr) or heat shock (55°C for 1 hr) of PyMT cells at 70-80% confluence. Blocking antibodies against TIM-3 (clone RMT3-23, BioLegend), Galectin-9 (clone RG9-1, BioXCell), HMGB1 (clone 3E8, BioLegend, dialyzed to remove sodium azide), or CEACAM-1 (clone MAb-CC1, BioLegend) were added to the supernatant at 10 μg/ml.

Transwell Assay

Splenic $CD8^+$ T cells were isolated by negative selection using the MojoSort Mouse $CD8^+$ T Cell Isolation Kit (Biolegend) following the manufacturer's instructions. Isolated cells were plated at $2x10^6$ per mL in RPMI 1640 containing 2.0 mM L-glutamine and 25 mM HEPES, supplemented with 10 mM Sodium Pyruvate, nonessential amino acids, 100 U/ml penicillin/streptomycin, 55 μM β-ME, and 10% fetal calf serum (complete media). Cells were stimulated with 1 μg/mL ionomycin (Invivogen) and 1 ng/mL phorbol myristate acetate (PMA, Invivogen) for 7 days, with complete media supplemented with 200 U/mL recombinant human IL-2 added on days 3 and 6. Following stimulation, cells were resuspended at $5x10^5$ per mL in RPMI 1640 supplemented with 0.1% bovine serum albumin, and were incubated at 4°C for 60 min with or without 100 nM (±)-AMG 487 (R&D Systems). Cells were then plated in the top well of 96 well transwell plate (3 μm polycarbonate membrane pore, Corning). The bottom well of the plate contained RPMI 1640 supplemented with 0.1% BSA, either with or without recombinant mouse CXCL9 or CXCL10 (Biolegend). Cells were allowed to migrate for 1 hr at 37°C, prior to data collection with a MACSQuant VYB flow cytometer (Miltenyi Biotech) and analysis using FlowJo version 10.

QUANTIFICATION AND STATISTICAL ANALYSIS

Statistical analyses were performed using Prism 6-7 (GraphPad). Data points represent biological replicates and are shown as the mean ± SEM unless otherwise indicated. Statistical significance was determined as indicated in the figure legends. For growth curves significance was determined via 2-way ANOVA with Tukey's multiple comparisons test, with significance shown for the final data point. A 2-way unpaired t-test or 2-way unpaired t-test with Welch's correction was used for comparison between groups with equal or unequal variance, respectively. Mann-Whitney and Kruskal-Wallis was used for data failing the D'Agostino & Pearson omnibus

normality test. Significance is shown as *$p < 0.05$, **$p < 0.01$, ***$p < 0.001$ as described in each figure legend. Heat maps were generated with GENE-E software (http://www.broadinstitute.org/cancer/software/GENE-E/), with hierarchical clustering performed with a one minus Pearson correlation. Linear regression analysis in breast cancer was performed in Prism using the dataset from The Cancer Genome Atlas Network (Cancer Genome Atlas Network, 2012). Gene expression data from fine needle aspirate obtained prior to neoadjuvant chemotherapy in breast cancer patients was obtained from 2 datasets (GSE20194, GSE20271) annotated for pathologic complete response (Hess et al., 2006; Tabchy et al., 2010). Survival analysis was performed using Kaplan-Meier Plotter (kmplot.com) (Gyorffy et al., 2010).

Cancer Cell, Volume *33*

Supplemental Information

TIM-3 Regulates CD103^{+} Dendritic Cell Function and Response to Chemotherapy in Breast Cancer

Álvaro de Mingo Pulido, Alycia Gardner, Shandi Hiebler, Hatem Soliman, Hope S. Rugo, Matthew F. Krummel, Lisa M. Coussens, and Brian Ruffell

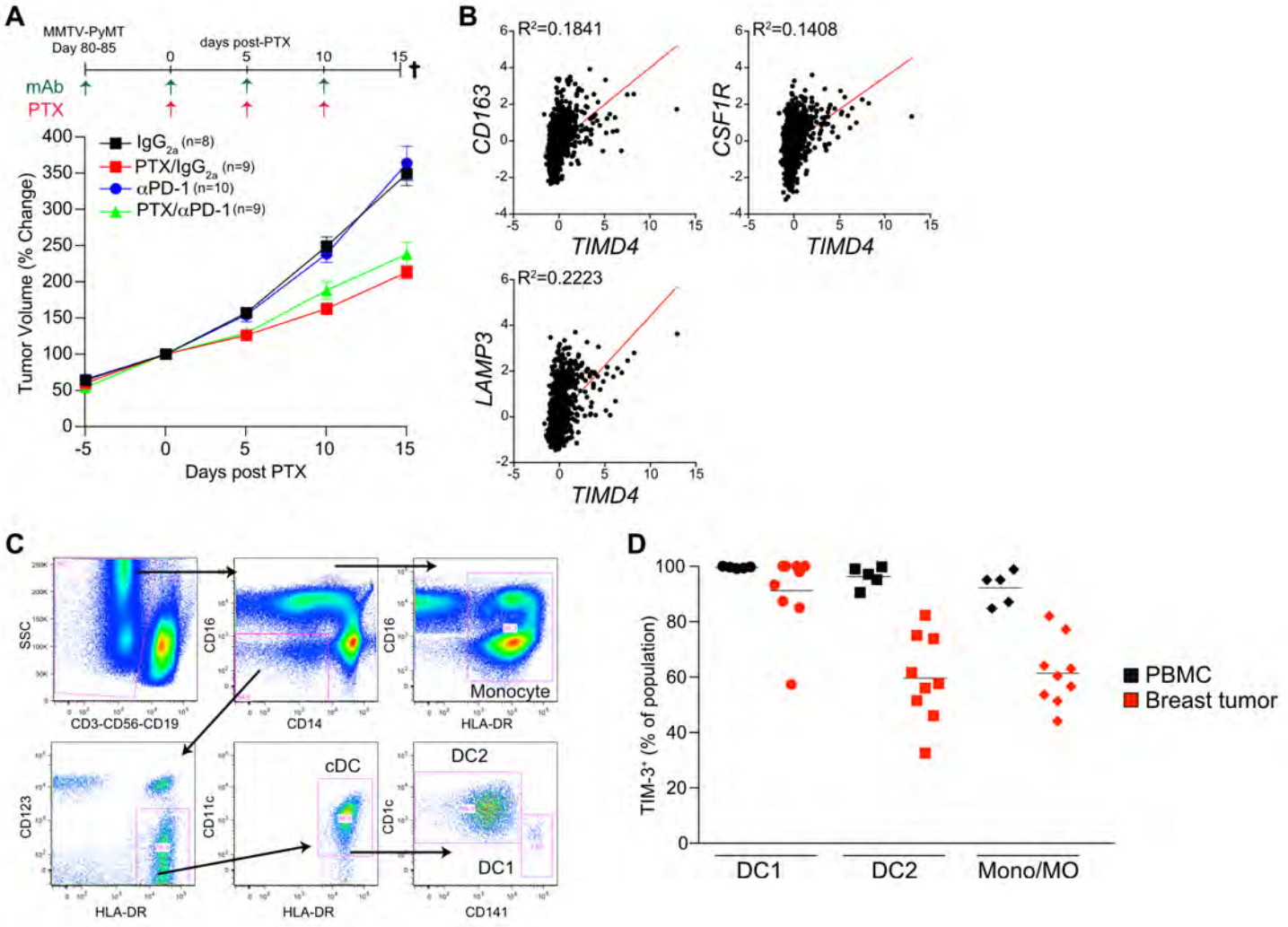

Figure S1, related to Figure 1

(A) Tumor volume shown as a relative change from the initiation of chemotherapy (day 0) in MMTV-PyMT animals. Mice were treated with an IgG_{2a} isotype control or αPD-1, alone or together with 10 mg/kg PTX as indicated. n=8-10 mice per group, pooled over 4 cohorts. Data are mean ± SEM. (B) Correlation between *TIMD4* expression and myeloid genes (*CD163*, *CSF1R*, *LAMP3*) in human breast cancer samples from the TCGA dataset (n=1161, R^2 values by linear regression). (C) Gating strategy for human DCs shown in a peripheral blood sample. (D) Percentage of TIM-3^+ cells within the $CD141^+$ cDC1, $CD1c^+$ cDC2 or $CD14^+$ monocyte/macrophage populations in the peripheral blood of healthy volunteers (n=5) or breast tumors (n=9). Horizontal bars represent the mean.

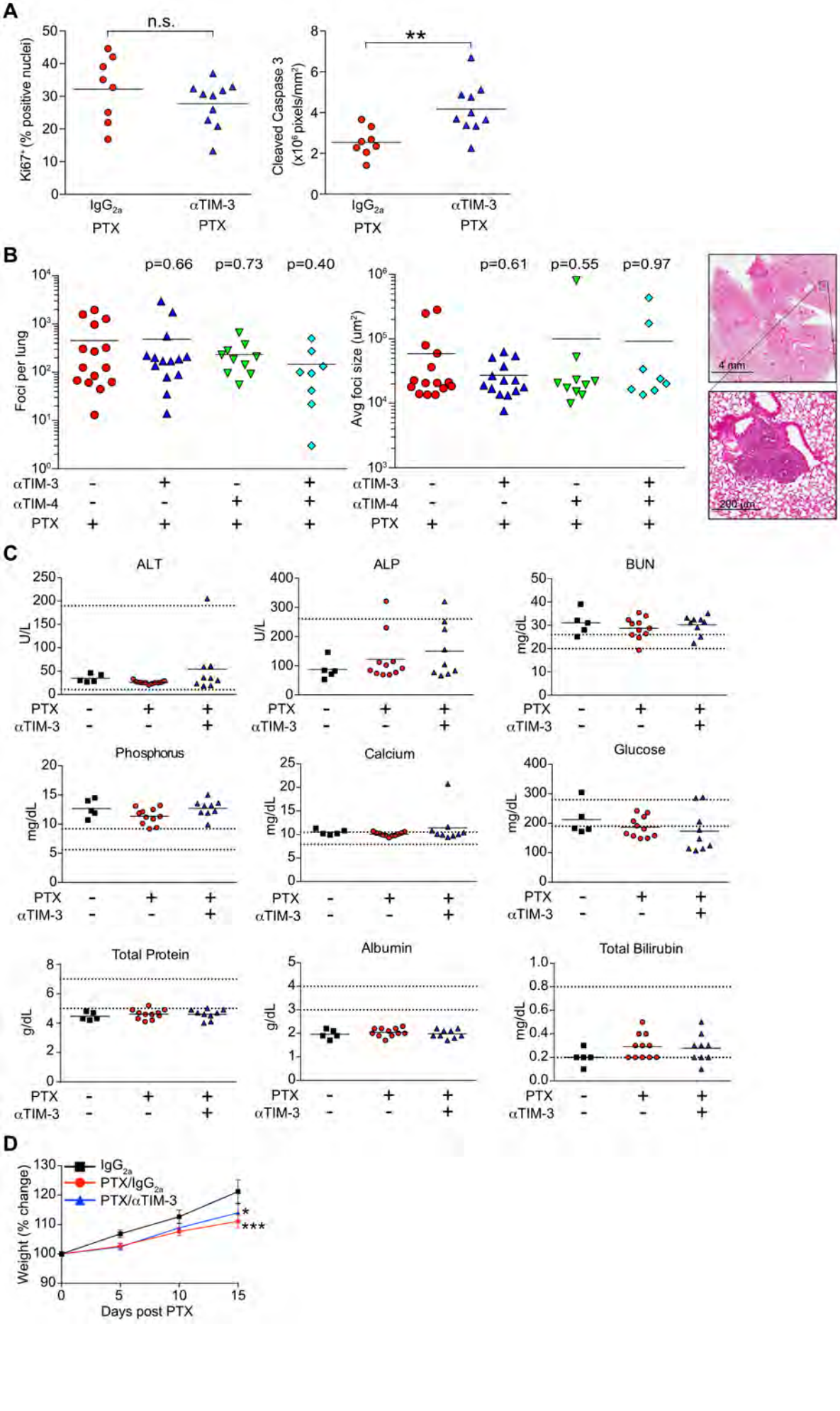
A
n.s.
**
Ki67+ (% positive nuclei)
Cleaved Caspase 3 (x10^6 pixels/mm^2)
IgG2a PTX
αTIM-3 PTX
B
p=0.66
p=0.73
p=0.40
p=0.61
p=0.55
p=0.97
Foci per lung
Avg foci size (um^2)
αTIM-3
αTIM-4
PTX
4 mm
200 um
C
ALT
ALP
BUN
Phosphorus
Calcium
Glucose
Total Protein
Albumin
Total Bilirubin
U/L
mg/dL
g/dL
D
IgG2a
PTX/IgG2a
PTX/αTIM-3
Weight (% change)
Days post PTX
*
***

Figure S2, related to Figure 2

(A) Automated analysis of Ki67 positive nuclei or cleaved caspase 3 immunohistochemistry staining in orthotopic PyMT tumors following treatment with IgG_{2a}/PTX or αTIM-3/PTX. n=8-10 per group, data pooled from 2 experiments. **p<0.01, significance determined by an unpaired t-test. (B) The frequency and size of metastatic foci in the lungs of MMTV-PyMT animals treated with αTIM-3, αTIM-4, or PTX. Representative images are shown to the right. n=8-16, pooled over 8 cohorts. p value shown compared to PTX alone, with significance determined by Mann-Whitney. (C) Metabolic function tests reflecting serum isolated from mice treated with IgG_{2a} alone, PTX/IgG_{2a}, or PTX/αTIM-3. Samples were taken by cardiac puncture at end-stage. Significance was determined by an unpaired t-test, with none found. The horizontal dotted lines indicate the expected range for healthy animals. ALT, alanine transaminase; ALP, alkaline phosphatase; BUN, blood urea nitrogen. (D) Weight of mice treated with IgG_{2a} alone, PTX/IgG_{2a}, or PTX/αTIM3. n=10 per group, pooled over 8 cohorts. Data are shown as the mean ± SEM; *p<0.05, ***p<0.001, with significance determined by 2-way ANOVA compared to IgG_{2a} control. Horizontal bars in A-C represent the mean.

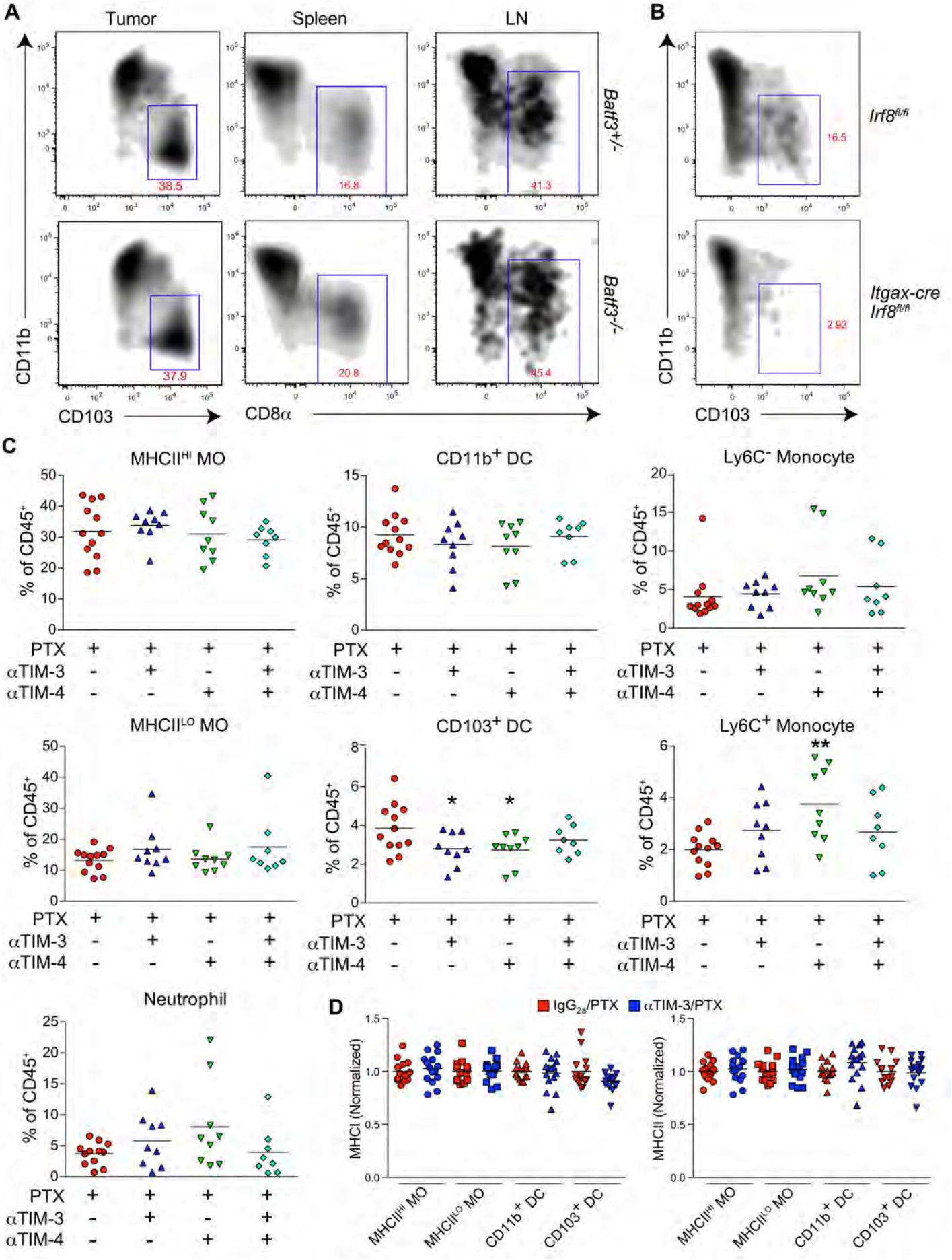
A
Tumor
Spleen
LN
Batf3+/-
Batf3-/-
38.5
16.8
41.3
37.9
20.8
45.4
CD11b
CD103
CD8α
B
Irf8fl/fl
Itgax-cre Irf8fl/fl
16.5
2.92
CD11b
CD103
C
MHCIIHI MO
CD11b+ DC
Ly6C- Monocyte
MHCIILO MO
CD103+ DC
Ly6C+ Monocyte
Neutrophil
% of CD45+
PTX
αTIM-3
αTIM-4
D
IgG2a/PTX
αTIM-3/PTX
MHCI (Normalized)
MHCII (Normalized)
MHCIIHI MO
MHCIILO MO
CD11b+ DC
CD103+ DC

Figure S3, related to Figure 3

(A) cDC subsets (gated on $CD45^+CD11c^+MHCII^+F4/80^-$) within MMTV-PyMT tumors from animals either proficient (+/-) or deficient (-/-) in *Batf3*, or from the spleen or lymph nodes (LN) of wild type FVBN/J animals either proficient or deficient in *Batf3*. One of two representative experiments shown. (B) cDC subsets (gated on $CD45^+CD11c^+MHCII^+F4/80^-$) within PyMT tumors implanted into chimeric C57BL/6J animals reconstituted with either *Itgax-cre;Irf8*$^{fl/fl}$ or *Irf8*$^{fl/fl}$ bone marrow. (C) Frequency of myeloid subsets as a percentage of total $CD45^+$ cells within MMTV-PyMT tumors of mice treated for 15 days with PTX and a combination of αTIM-3 and/or αTIM-4 antibodies. n=8-12 per group, data pooled over 7 cohorts. *$p<0.05$, **$p<0.01$, with significance determined by unpaired t-test with Welch's correction compared to PTX alone group. (D) Surface expression of MHCI and MHCII on macrophages and cDCs from MMTV-PyMT animals treated with PTX for 7 days in conjunction with either IgG_{2a} or αTIM-3. n=13-15 per group with data pooled over 3 experiments by normalizing to 1. Horizontal bars in C, D represent the mean.

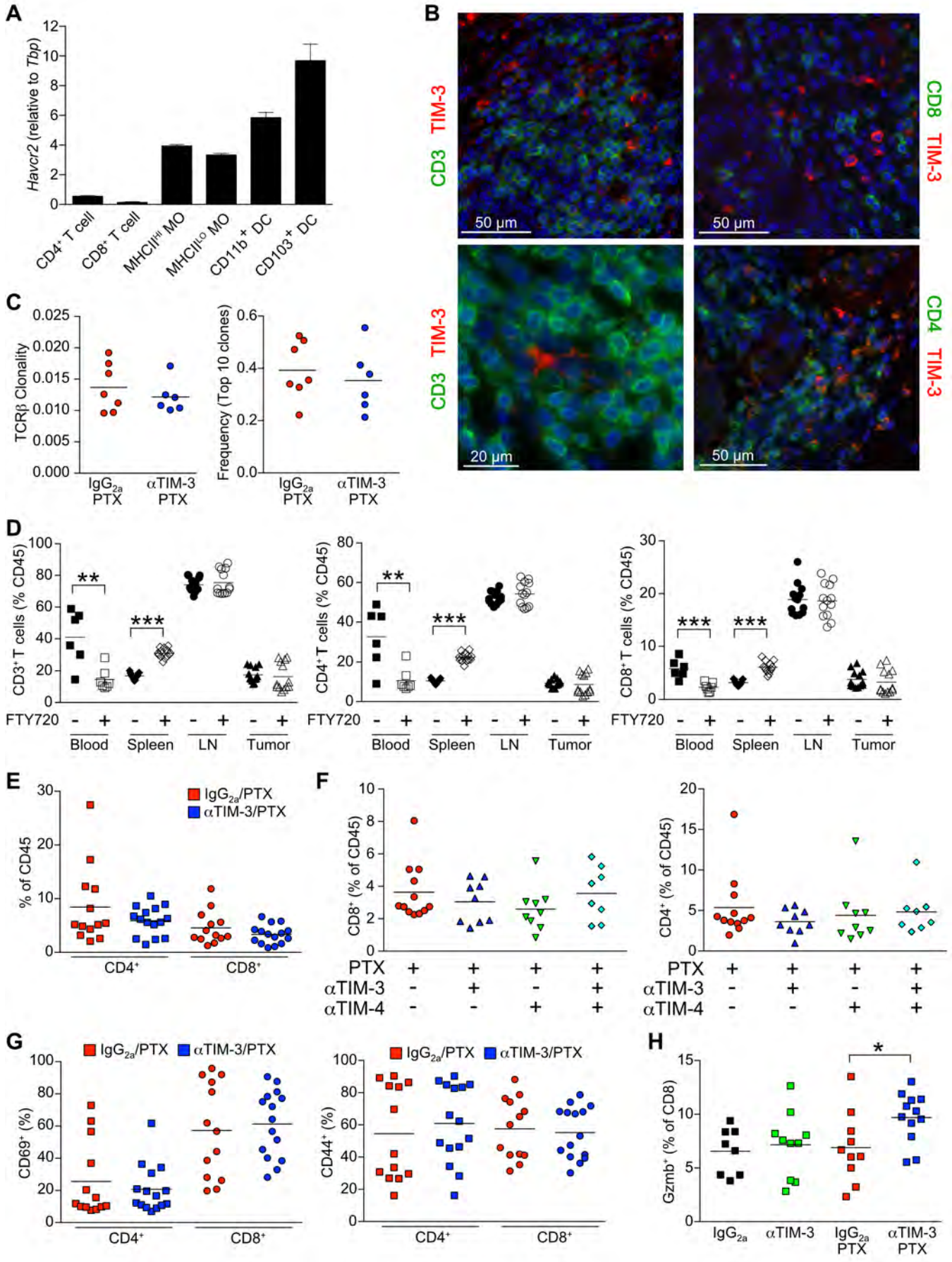
A
Havcr2 (relative to Tbp)
CD4+ T cell
CD8+ T cell
MHCIIHI MO
MHCIILO MO
CD11b+ DC
CD103+ DC
B
CD3 TIM-3
CD8 TIM-3
CD3 TIM-3
CD4 TIM-3
50 μm
20 μm
C
TCRβ Clonality
Frequency (Top 10 clones)
IgG2a PTX
αTIM-3 PTX
D
CD3+ T cells (% CD45)
CD4+ T cells (% CD45)
CD8+ T cells (% CD45)
FTY720
Blood
Spleen
LN
Tumor
E
IgG2a/PTX
αTIM-3/PTX
% of CD45
CD4+
CD8+
F
CD8+ (% of CD45)
CD4+ (% of CD45)
PTX
αTIM-3
αTIM-4
G
CD69+ (%)
CD44+ (%)
H
Gzmb+ (% of CD8)
IgG2a
αTIM-3
IgG2a PTX
αTIM-3 PTX

Figure S4, related to Figure 4

(A) *Havcr2* mRNA expression levels in leukocyte populations isolated from MMTV-PyMT mice treated with PTX, as determined by real time PCR. Data are normalized to *Tbp* expression and displayed as mean ± SEM with n=6-8 per cell type. (B) Immunofluorescent staining for TIM-3 (red) and CD3, CD4 or CD8 (green) in human breast cancer. DNA was visualized with Hoechst 33342 (blue). 3 patient samples were analyzed for each combination. (C) Clonality of T cell receptor β (TCRβ) in the peripheral blood of MMTV-PyMT mice treated with αTIM-3 and PTX (day 15), as determined by immunoSEQ. n=6-7 per group, data pooled over 2 cohorts. (D) Percentage of $CD3^+$, $CD3^+CD4^+$ or $CD3^+CD8^+$ T cells within the lymph nodes (LN), spleens, and tumors of animals bearing implanted tumors treated with DMSO or FTY720 for 7 days. Data merged from 3 experiments. (E) Frequency of $CD8^+$ and $CD4^+$ T cells within MMTV-PyMT tumors as a percent of total $CD45^+$ cells 2 days following the 2nd dose of PTX (day 7). n=13-15 mice per group pooled over 3 cohorts. (F) Frequency of $CD8^+$ and $CD4^+$ T cells within MMTV-PyMT tumors as a percent of total $CD45^+$ cells (day 15). n=8-12 per group, data pooled over 7 cohorts (G) Percent of T cells expressing CD69 (left) or CD44 (right) within MMTV-PyMT tumors, 2 days post PTX (day 7). n=13-15 mice per group pooled over 3 cohorts. (H) $CD8^+Gzmb^+$ T cells shown as percentage of total $CD8^+$ T cells. Data are from mice bearing PyMT implantable tumors treated with IgG_{2a} isotype control, αTIM-3, or PTX. Tumors were analyzed 2 days post PTX (day 7). n=8-12 per group, data pooled from 2 experiments. Horizontal bars in C-H represent the mean; *$p<0.05$, **$p<0.01$, ***$p<0.001$ by an unpaired t-test.

A

MHCII^{HI} MOs		
Gene	Fold	p value
Ccl7	1.7976	0.0015
Hcst	1.7330	0.0481
Irf7	0.6562	0.0069
Tlr5	0.6477	0.0102
Cxcl1	0.6376	0.0045
Cd34	0.6036	0.0366
Ifitm1	0.5872	0.0106
Il1r2	0.3914	0.0010

CD11b^{+} DCs		
Gene	Fold	p value
Traf2	2.6839	0.0022
Cxcl9	2.5956	0.0141
Cd22	2.5538	0.0029
Cxcl11	1.9942	0.0237
Cx3cr1	1.8214	0.0071
Pdgfb	1.8168	0.0008
Fcgr4	1.7617	0.0355
Cxcl10	1.6686	0.0311
Ccl3	1.6685	0.0305
Vcam1	1.6580	0.0356
Tnfsf13b	1.6482	0.0425
Tlr1	1.6399	0.0371
Cd69	1.6384	0.0144
Tgfbr1	1.5793	0.0087
Cmklr1	1.5758	0.0142
Irf8	1.5616	0.0120
Trem2	1.5530	0.0474
Tnfrsf14	1.5506	0.0430
Ccl12	1.5366	0.0186
C1qa	1.5204	0.0300
Cd40	1.5066	0.0051
Tlr5	0.6409	0.0344
Fkbp5	0.6153	0.0040

MHCII^{LO} MOs		
Gene	Fold	p value
Cd3eap	2.5285	0.0425
Gata3	2.2161	0.0025
Ltf	2.2066	0.0087
Zbtb7b	2.0216	0.0496
Bcl2	1.9110	0.0079
Rorc	1.8199	0.0012
Smad5	1.7975	0.0076
Casp2	1.7947	0.0148
Ptk2	1.7739	0.0471
Abcb10	1.7576	0.0047
Il15ra	1.7369	0.0257
S100a8	1.7351	0.0302
Muc1	1.6901	0.0346
Cd24a	1.6558	0.0047
C3	1.6094	0.0000
Rela	1.6025	0.0441
Il6st	1.5794	0.0066
Psmd7	1.5782	0.0405
Stat5a	1.5377	0.0112
Pdcd2	1.5259	0.0193
Ccl12	0.6253	0.0435
Ifngr2	0.6061	0.0143
Cxcl1	0.6008	0.0393
Clec4e	0.5897	0.0451
Msr1	0.5672	0.0453
Ifit2	0.5576	0.0155
Crlf2	0.5559	0.0281
Fcgr2b	0.4848	0.0386
Trem1	0.4236	0.0350
Ifitm1	0.4209	0.0078

CD103^{+} DCs		
Gene	Fold	p value
Cxcl11	2.5306	0.0037
Cxcl10	1.9417	0.0201
Cxcl9	1.6854	0.0440
Tagap	1.5823	0.0181
Cd40	1.5252	0.0243

B

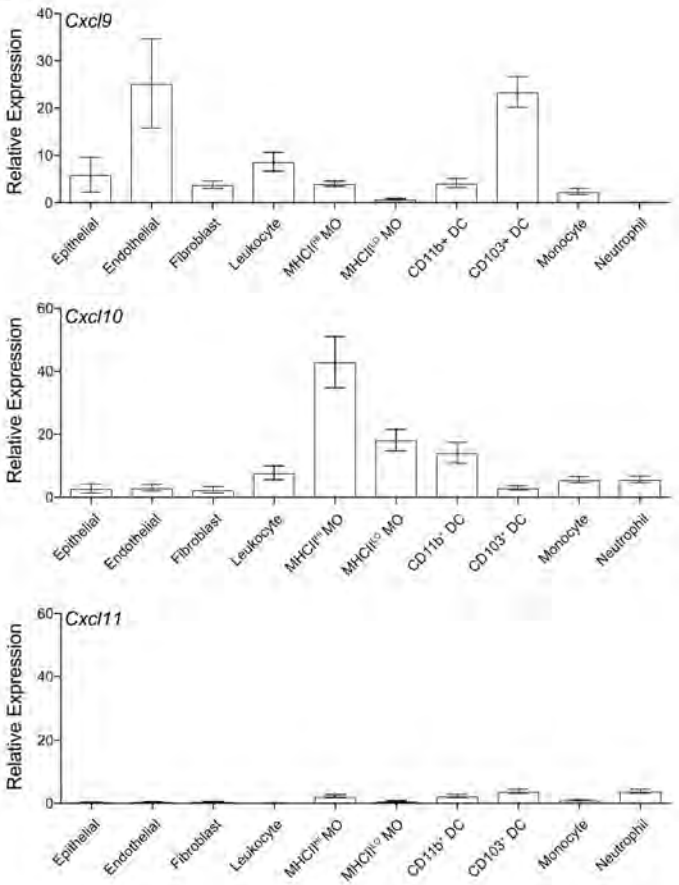

C

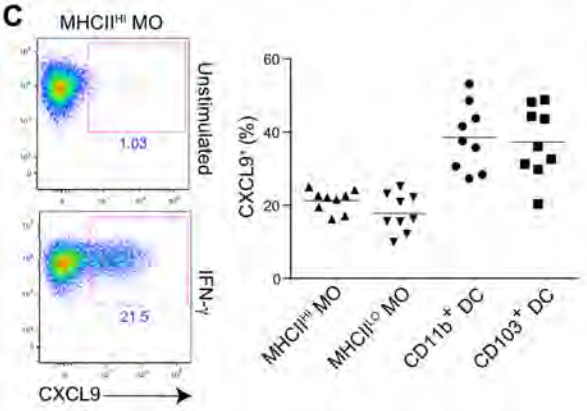

D

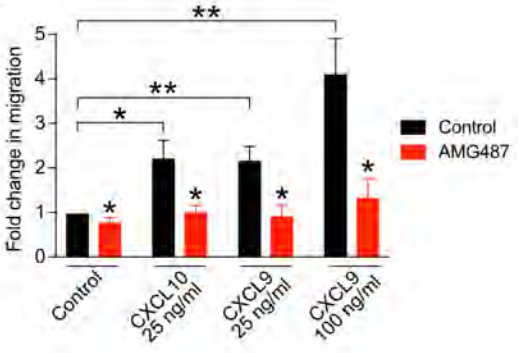

Figure S5, related to Figure 5

(A) Fold change in mRNA expression levels in tumor macrophages and cDCs isolated from mice bearing orthotopically implanted PyMT tumors 2 days following second dose of PTX (day 7). Expression was determined by NanoString. Significance was determined by an unpaired t-test, with data pooled from 2 experiments. (B) mRNA expression of *Cxcl9, Cxcl10*, or *Cxcl11* by epithelial and stromal cells in untreated MMTV-PyMT tumors. Data are normalized to *Tbp* expression and displayed as mean ± SEM with n=8 per cell type. (C) Percentage of MMTV-PyMT tumor macrophages and cDCs expressing CXCL9 following ex vivo stimulation with 40 ng/ml IFN-γ for 4 hr in the presence of brefeldin A. Representative intracellular staining is shown to the left. Horizontal bars represent the mean (n=9), with data pooled from two experiments. (D) Transwell migration of activated $CD8^+$ splenic T cells in response to recombinant murine CXCL9 or CXCL10, either in the presence or absence of 100 nM of the CXCR3 inhibitor (±)-AMG 487. Normalized data are displayed as mean ± SEM of biological replicates compiled from three independent experiments. Significance was determined by an unpaired t-test, with *$p<0.05$, **$p<0.01$.

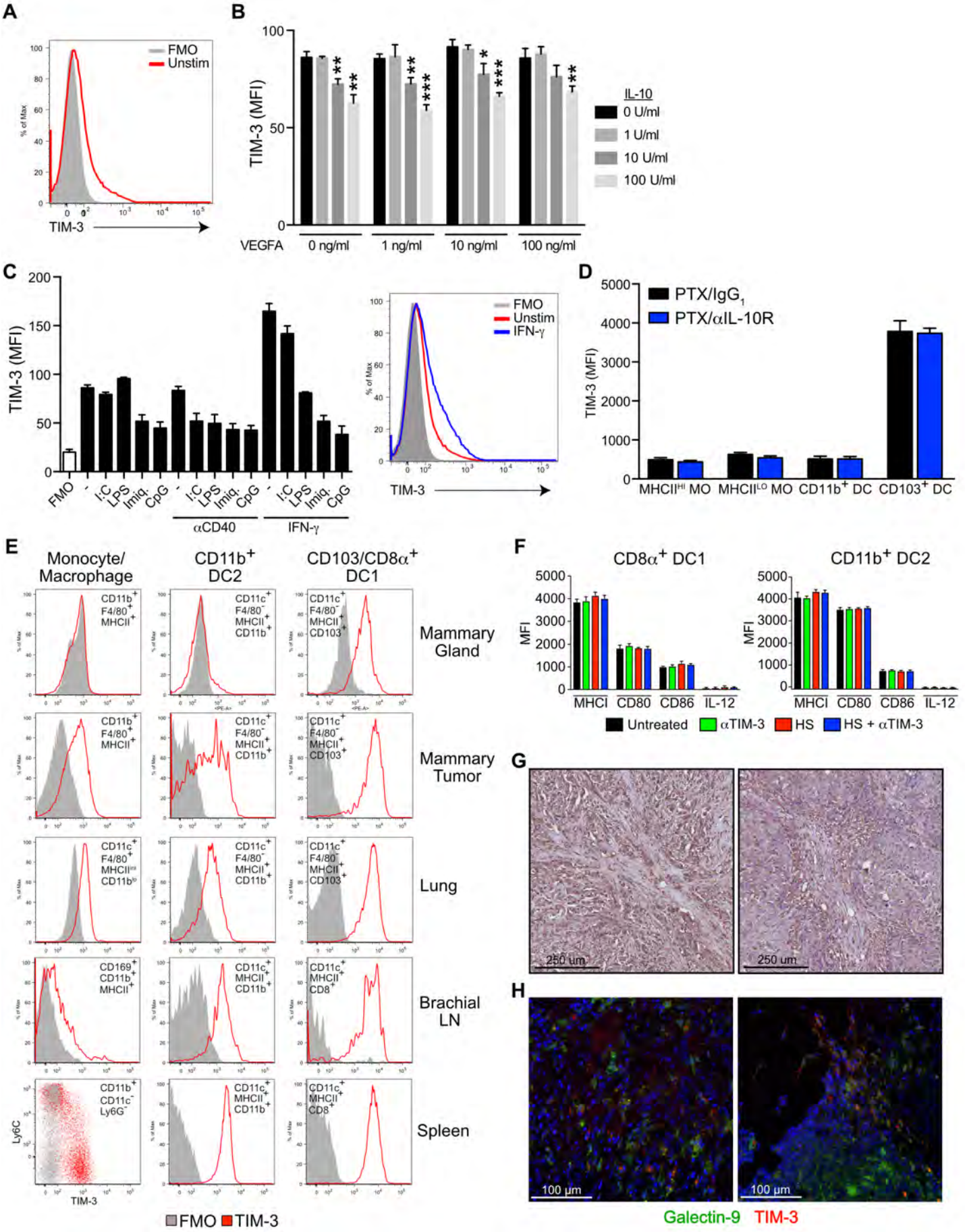
A
FMO
Unstim
% of Max
TIM-3
B
TIM-3 (MFI)
IL-10
0 U/ml
1 U/ml
10 U/ml
100 U/ml
VEGFA
0 ng/ml
1 ng/ml
10 ng/ml
100 ng/ml
C
TIM-3 (MFI)
FMO
-
I:C
LPS
Imiq.
CpG
αCD40
IFN-γ
Unstim
TIM-3
D
PTX/IgG1
PTX/αIL-10R
TIM-3 (MFI)
MHCIIHI MO
MHCIILO MO
CD11b+ DC
CD103+ DC
E
Monocyte/ Macrophage
CD11b+ DC2
CD103/CD8α+ DC1
Mammary Gland
Mammary Tumor
Lung
Brachial LN
Spleen
Ly6C
TIM-3
FMO
TIM-3
F
CD8α+ DC1
CD11b+ DC2
MFI
MHCI
CD80
CD86
IL-12
Untreated
αTIM-3
HS
HS + αTIM-3
G
250 μm
H
100 μm
Galectin-9
TIM-3

Figure S6, related to Figure 6

(A-C) Surface expression of TIM-3 on FLT-3L-induced BMDCs as measured by flow cytometry, either unstimulated or stimulated with the indicated conditions for 24 hr. (A) Histogram displaying TIM-3 surface expression relative to fluorescence minus one (FMO) control. (B) TIM-3 surface mean fluorescence intensity (MFI) following incubation with IL-10 or VEGFA. (C) TIM-3 surface MFI following stimulation with Poly(I:C), LPS, Imiquimod, CpG, αCD40, or IFN-γ. A representative histogram is shown on the right. Data for B-C are displayed as mean ± SD of technical replicates; *$p<0.05$, **$p<0.01$, ***$p<0.001$, significance determined by an unpaired t-test. One of two representative experiments is shown. (D) TIM-3 surface MFI on macrophage and cDC subsets from tumors of MMTV-PyMT mice treated with PTX and either IgG_1 isotype control or αIL-10R antibody. n=7 per group, data shown as mean ± SEM. (E) Surface expression of TIM-3 in monocytes, macrophages, $CD11b^+$ cDCs, and $CD103^+/CD8^+$ cDCs in the mammary gland, lung, spleen and lymph nodes (LNs) of non-tumor bearing animals. n=4, one of two representative experiments shown. (F) Expression of activation markers by splenic cDCs following incubation with αTIM-3 and/or tumor cell debris generated by heat shock (HS). One of two representative experiments is shown, with data displayed as mean ± SD of 4 technical replicates. (G) Representative galectin-9 immunohistochemistry in human breast cancer samples (n=5). (H) Representative immunofluorescent staining for TIM-3 (red) and galectin-9 (green) in human breast cancer. DNA was visualized with Hoechst 33342 (blue). 3 patient samples were analyzed for each combination.

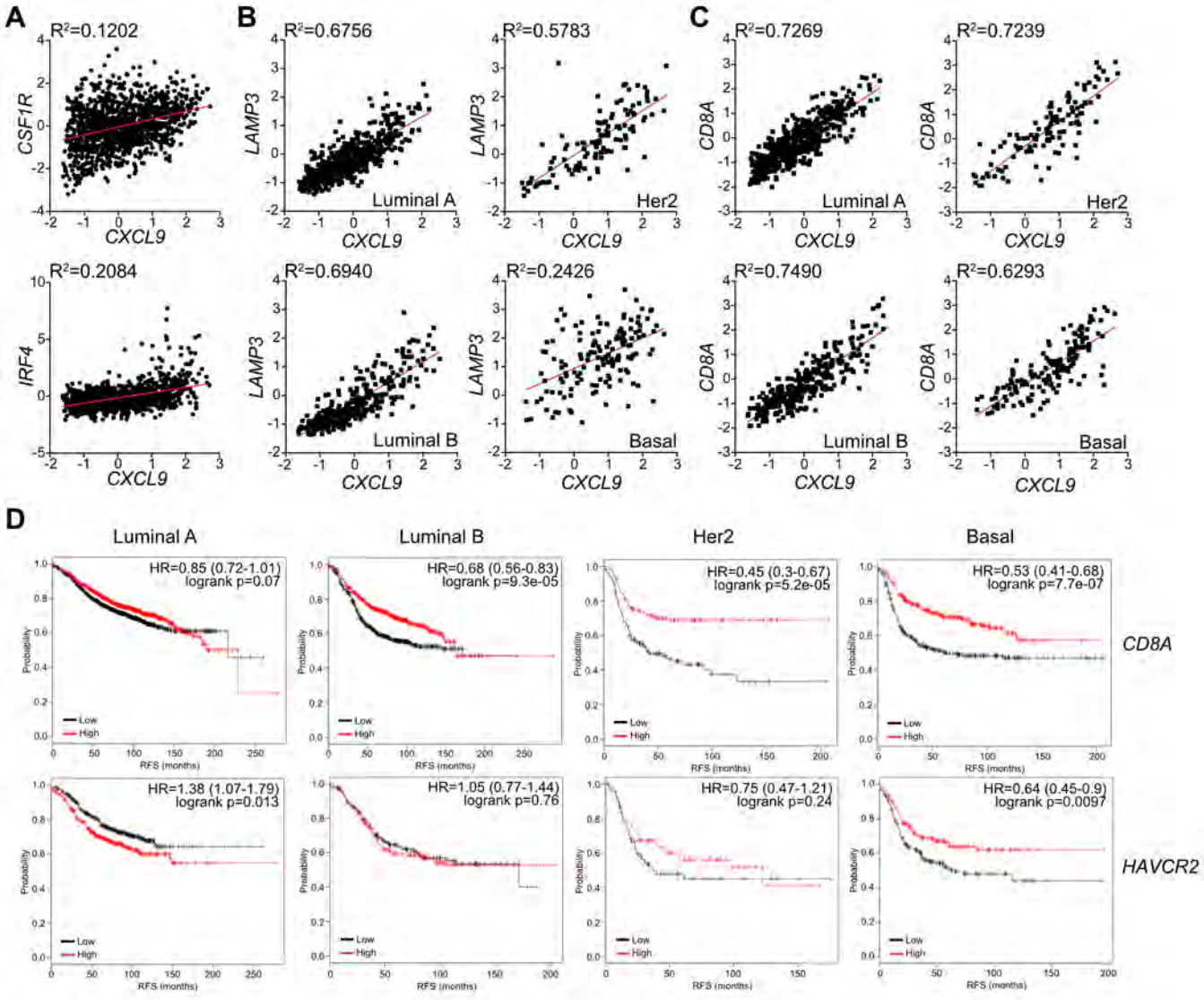

Figure S7, related to Figure 7

(A) Linear regression analysis between *CXCL9* expression and *CSF1R* or *IRF4* in human breast cancer samples from the TCGA dataset (n=1161). (B-C) Linear regression analysis between *CXCL9* expression and (B) *LAMP3* or (C) *CD8A* in samples from intrinsic luminal A (n=513), luminal B (n=286), Her2 (n=112) and basal (n=145) molecular subtypes. (D) Recurrence free survival (RFS) based upon median expression of *CD8A* or *HAVCR2* in breast tumor tissue. Data are shown for intrinsic luminal A, luminal B, Her2 and basal molecular subtypes (n=1933, 1149, 251, 618 for *CD8A*; n=841, 407, 156, 360 for *HAVCR2*). Hazard ratio (HR) and logrank p values are shown in the upper right of each Kaplan-Meier Plot.